

DETERMINATION OF POOL BOILING CRITICAL HEAT FLUX ENHANCEMENT IN
NANOFLUIDS

by

Bao H. Truong

SUBMITTED TO THE DEPARTMENT OF NUCLEAR SCIENCE
AND ENGINEERING
IN PARTIAL FULFILLMENT OF THE REQUIREMENTS FOR THE DEGREE OF
BACHELOR OF SCIENCE IN NUCLEAR SCIENCE AND ENGINEERING
AT THE
MASSACHUSETTS INSTITUTE OF TECHNOLOGY

MAY 2007
[June 2007]

Bao H. Truong. All rights reserved.

The author hereby grants to MIT permission to reproduce and to distribute publicly
Paper and electronic copies of this thesis document in whole or in part.

Signature of Author: _____

Department of Nuclear Science and Engineering

May 11th 2007

Certified by _____

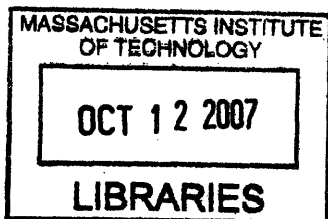
Jacopo Buongiorno
Assistant Professor of Nuclear Science and Engineering
Thesis Supervisor

Certified by _____

Lin-Wen Hu
Associate Director, Nuclear Reactor Laboratory
Thesis Supervisor

Accepted by: _____

David G. Cory
Professor of Nuclear Science and Engineering
Chairman, NSE Committee for Undergraduate Students



ARCHIVES

DERTERMINATION OF POOL BOILING CRITICAL HEAT FLUX ENHANCEMENT IN
NANOFLUIDS

by

Bao H. Truong

Submitted to the Department of Nuclear Science and Engineering on May 11th 2007
In Partial Fulfillment of the Requirements for the Degree of
Bachelor of Science in Nuclear Science and Engineering

ABSTRACT

Nanofluids are engineered colloids composed of nano-size particles dispersed in common fluids such as water or refrigerants. Using an electrically controlled wire heater, pool boiling Critical Heat Flux (CHF) of Alumina and Silica water-based nanofluids of concentration less than or equal to 0.1 percent by volume were measured. Silica nanofluids showed CHF enhancement up to 68% and there seems to be a monotonic relationship between nanoparticle concentration and magnitude of enhancement. Alumina nanofluids had CHF enhancement up to 56% but the peak occurred at the intermediate concentration. The boiling curves in nanofluid were found to shift to the left of that of water and correspond to higher nucleate boiling heat transfer coefficients in the two-phase flow regime. SEM images show a porous coating layer of nanoparticles on wires subjected to nanofluid CHF tests. These coating layers change the morphology of the heater's surface, and are responsible for the CHF enhancement. The thickness of the coating was estimated using SEM and was found ranging from 3.0 to 6.0 micrometers for Alumina, and 3.0 to 15.0 micrometers for Silica. Inductively Coupled Plasma Spectroscopy (ICP-OES) analyses were also attempted to quantify the mass of the particle deposition but the results were inconsistent with the estimates from the SEM measurement.

Thesis Supervisor: Jacopo Buongiorno

Title: Assistant Professor of Nuclear Science and Engineering

Thesis Supervisor: Lin-Wen Hu

Title: Associate Director of the MIT Nuclear Reactor Laboratory

ACKNOWLEDGMENTS:

First, I would like to thank Professor Jacopo Buongiorno and Dr. Lin-wen Hu, my thesis advisors, for their support and guidance. Their advices, questions and inputs were useful and important for this project. In addition, I want thank Dr. Thomas McKrell who helped me with the experiments all this time. His suggestions, especially for the post CHF experiment analyses, were always valuable. Also, I want to thank graduate student Sung Joong Kim, with whom I had many insightful discussions. Thank you to Eric Forrest, my undergraduate fellow, who helped me with the particle's size measurement. Finally, I want to thank my family, and all my friends, especially Jennifer Choy, who have always been there and have supported me for the last four years.

Table of Contents:

1	Chapter 1 - Introduction	7
1.1	Background	7
1.2	Recent Work in CHF of Nanofluids.....	8
2	Chapter 2 – Properties of Nanofluids.....	10
2.1	Preparation of Nanofluids	10
2.2	Nanofluids Characterization.....	10
3	Chapter 3 – Critical Heat Flux Mechanisms	17
4	Chapter 4 – CHF Experiments and Results.....	20
4.1	CHF Experiment Set Up and Procedure.....	20
4.1.1	Experimental Set Up	20
4.1.2	CHF Measurement Procedure	21
4.2	Results	23
4.2.1	CHF in Alumina Nanofluids	23
4.2.2	CHF in Silica Ludox TMA Nanofluids.....	28
5	Chapter 5 – Characterization of Heater’s Surface.....	31
5.1	SEM Characterization	31
5.1.1	Wires in Alumina Nanofluids.....	31
5.1.2	Wires in Silica Nanofluids	37
5.2	Analyses	42
5.2.1	Mechanism for Particle Deposition.....	42
5.2.2	Thickness of Nanoparticle Deposition	43
5.2.3	Possible CHF Enhancement Mechanisms.....	46
5.2.4	Nucleate Boiling Heat Transfer Coefficient.....	48
6	Chapter 6 – Conclusion	50

List of Figures:

Figure 2-1: Schematic set up for DLS	11
Figure 2-2: XRD spectrum of 20 w% Alumina nanofluid.	15
Figure 3-1: Typical boiling curve.....	17
Figure 4-1 : CHF pool boiling experiment facility set up	20
Figure 4-2: An example of current input through the stainless steel 316 wire heater for CHF measurement of Alumina nanofluid.	22
Figure 4-3: CHF Data for different dimensionless radius, R'	24
Figure 4-4: CHF values in Alumina of different volume concentration.	25
Figure 4-5: Boiling curves for Alumina nanofluids of different volume concentration and of water with bare stainless steel wire and pre-coated wire.	26
Figure 4-6: Heat transfer coefficient as a function of heat flux.	27
Figure 4-7: CHF in Silica nanofluids.	28
Figure 4-8: Boiling curves in Silica nanofluids, water and the Rohsenow correlation.....	29
Figure 4-9: Heat transfer coefficients in Silica nanofluids.....	30
Figure 5-1: SEM image of stainless steel wires after CHF experiments.....	31
Figure 5-2: SEM images (200x magnification) of wires in Alumina nanofluids.....	33
Figure 5-3: Comparison between SEM images (200x magnification) of wire in 0.01v% Alumina (A) and pre-coated wires in deionized water (B, C, D).....	34
Figure 5-4: SEM image (3500x) of stainless steel in 0.1%v Alumina with EDS spectra.....	35
Figure 5-5: Wire is mounted vertically on SEM mounting plate in order for the thickness of the nanoparticle deposition can be approximately measured.	36
Figure 5-6: Approximate thickness of coating layer on wires in Alumina nanofluids of different concentration.	36
Figure 5-7: Stainless steel wire tested in 0.001vol% Silica with EDS and thickness measurement.....	37
Figure 5-8: SEM of wires in 0.01 vol% Silica (left figures) and 0.1v% Silica (right figures).	38
Figure 5-9: Vertical view of wire in 0.01 vol% with thickness measurement and EDS to identify elemental composition.	39
Figure 5-10: SEM of wire view from vertical at different locations.....	40
Figure 5-11: SEM images of two pre-coated (via nucleation boiling in 0.1 vol% Silica nanofluids) wires with Silica in water CHF tests.	41
Figure 5-12: SEM image of wires after CHF experiment in Silica nanofluids.....	42
Figure 5-13: Theoretical calculation for mass of nanoparticle deposited on wire.	44

List of Tables:

Table 2-1: Size and pH of nanoparticle in Silica and Alumina nanofluids 12

Table 2-2: Kinematic viscosity, thermal conductivity, and surface tension of Alumina nanofluids and water.. 13

Table 2-3: Kinematic viscosity, thermal conductivity, and surface tension of Silica nanofluids and water.. 13

Table 4-1: CHF experimental matrix 21

Table 5-1: ICP results. 45

Nomenclature:

<i>a</i>	area of vapor channel
<i>C</i>	constant in Zuber relation
<i>d</i>	diameter (m)
<i>f</i>	amount of water (ml)
<i>g</i>	gravitational constant (m/s ²)
<i>h_c</i>	heat transfer coefficient (W/m ² °C)
<i>h_{fg}</i>	latent heat of vaporization(J/kg)
<i>I</i>	current (A)
<i>L</i>	length of wire (m)
<i>m</i>	mass (kg)
<i>n</i>	amount of <i>x</i> w% nanofluid (ml)
<i>q</i>	heat flux (W/m ²)
<i>R</i>	radius (m)
<i>R'</i>	non-dimensional radius
<i>r</i>	resistance (ohm)
<i>t</i>	thickness of coating (μm)
<i>T</i>	temperature (°C)
<i>V</i>	voltage (V)
<i>v</i>	Specific volume(m ³ /kg)
<i>x</i>	weight percent of nanofluid
<i>y</i>	volume percent of nanofluid
<i>α</i>	temperature Coefficient of Resistance (1/°C)
<i>λ</i>	wavelength (m)
<i>ρ</i>	density (g/cm ³)
<i>σ</i>	surface tension (mN/m)

Subscript:

<i>br</i>	break through
<i>f</i>	liquid
<i>g</i>	vapor
<i>max</i>	maximum heat flux
CHF	Critical Heat Flux
<i>p</i>	particle
<i>RT</i>	Rayleigh-Taylor
<i>s</i>	saturation
<i>w</i>	water
<i>Z</i>	Zuber

Abbreviations:

CHF	Critical Heat Flux
DLS	Dynamic Light Scattering
EDS	Energy Dispersive Spectroscopy
ICP	Inductively Coupled Plasma
OES	Optical Emission Spectroscopy
SEM	Scanning Electron Microscopy
XRD	X-ray Diffraction

1 Chapter 1 - Introduction

1.1 Background

Important goals of reactor research are to increase power density, efficiency, to reduce waste production and to provide inherent safety. Achievements of these goals require work in many different fields. The Generation IV nuclear reactor systems have been the main focus in reactor research for the past several years. Research [1] has been initiated to contribute to the current development of Generation IV systems: Gas-Cooled Fast Reactors (GFR), Very-High Temperature Reactors (VHTR), Supercritical-Water-Cooled Reactors (SCWR), Sodium-Cooled Fast Reactors (SFR) and Lead-Cooled Fast Reactors (LFR). Some important research areas for these reactors include thermal hydraulics, nuclear fuel material, power conversion systems, coolant materials and waste management processes [1]. Generation IV nuclear systems are expected to provide a sustainable, safe, and competitive nuclear energy that is also proliferation-resistant. Overall this will contribute in solving the possible energy crisis in the future.

The Department of Nuclear Science and Engineering at the Massachusetts Institute of Technology has actively participated in the Generation IV and other advanced R&D programs. Research is being done on the pebble-bed reactor concepts, advance light water reactors as well as fuel materials. One of the current major research projects focuses in the department is study of the feasibility of the nuclear applications of nanofluids, i.e., engineered colloids of nano-size particles suspended in common fluids [2]. Buongiorno et al.[3] reported possible uses of nanofluids as primary coolant for Pressurized Water Reactor (PWR), in the accumulators and safety injection for Emergency Core Cooling Systems (ECCS), or for reactor cavity flooding. Besides reactors, many other industrial applications, such as electronic components, require coolant systems to remove heat from heated surfaces. High heat flux from these surfaces can be transferred to the coolant effectively via nucleate boiling. However, there is a point at which nucleate boiling can no longer transfer heat effectively due to

the transition to film boiling. The value of heat flux at this point is known as Critical Heat Flux (CHF). Increase in CHF can help raising a system's overall power density since the CHF value is proportional to the maximum amount of heat transfer by nucleate boiling. This subsequently improves the system's overall efficiency, reduces the cost of operation and provides a greater safety margin. The CHF enhancement capabilities of nanofluids in pool boiling and their mechanisms are investigated in this study.

1.2 Recent Work in CHF of Nanofluids

One of the most interesting properties of nanofluids is their boiling heat transfer behaviors [4] and research in CHF of nanofluids has only been of interest for the last several years. The term "nanofluid" was first introduced by Choi [5], who studied their possible enhancement in thermal conductivity. The nanoparticles (diameter < 100nm) dispersed in common fluids can be metal oxides (Alumina, Zirconia, Silica, etc...), metals (gold, silver, copper etc...), or other materials such as diamond, carbon nanotube or Teflon. While there are some discrepancies in the boiling heat transfer reported in the literature, all have observed enhancement in CHF of nanofluids compared to water, some as high as 200%. For example, Vassallo et al. [6] reported 60% CHF enhancement in Silica (SiO_2) nanofluid with particle of 10 to 50 nm diameter. Similarly, You et al. [2] showed 200% CHF enhancement in 0.005g/L Alumina (Al_2O_3) nanofluids. Kim et al. [7] also saw 200% increase in CHF in TiO_2 nanofluids with volume concentration from 10^{-5} to 10^{-1} percent. Kumar et al. [8] measured 50% CHF enhancement in Silica (SiO_2), Ceria (CeO_2) and Alumina (Al_2O_3). Bang and Chang [4] observed CHF enhancement in heaters arranged vertically and horizontally in Alumina nanofluid. Finally, Wen and Ding [9] reported up to 40% higher CHF for 1.25 w% particle loading. All of these are pool boiling CHF experiments using wire and/or flat plate heaters.

Furthermore, coating of nanoparticles deposited on the heating surfaces was also reported. Kim et al. [7] observed nanoparticle coating of the heater surface dependent on the particle loading in the nanofluids. Kumar et al. [8] found the surface roughness of the wire

changed after CHF experiment in nanofluids, possibly due to oxidation. Kumar et al. [8] also used Energy Dispersive Spectroscopy (EDS) to confirm the elemental composition of the nanoparticle coating. Bang and Chang [4] suggested the altered surface characteristic of the heater affects the heat transfer. Das et al. [10] saw a negative shift in boiling curves in nanofluid compare to that of water, while You et al. [2] did not see any change in the nucleate boiling heat transfer coefficients in nanofluids. However, only few attempts and little progress have been made in explaining pool boiling CHF enhancement mechanism in nanofluids [11]. Kim et al. [11] were the first to characterize the heater surface and to suggest a possible mechanism, which includes the increase in surface roughness of heater due to deposition of nanoparticles. This increase in surface roughness enhances the wettability of the heater, subsequently raising CHF. The mechanism proposed by Kim et al. [11] seems to capture results reported in literature. However, more experimental data are needed in order to confirm such mechanism.

In this work, pool boiling CHF enhancement in nanofluids was studied. However, contact angle was not measured because the heater was a wire of small diameter. Therefore, we will not be discussing effects of wettability on CHF either. The pool boiling CHF in Alumina (Al_2O_3) and Silica (SiO_2) nanofluids of volume concentration less than or equal to 0.1 vol%, with a stainless steel wire heater were first determined. The properties of the nanofluids used in CHF experiment, such as thermal conductivity, surface tension, and particle size distribution, were also measured. A thorough heater's surface characterization was done using SEM. The approximate thickness of the deposition of the particle was estimated to gain an insight of the amount of the deposited particles. This provides an approximation for surface roughness, which affects CHF. Inductively Coupled Plasma – Optical Emission Spectroscopy (ICP – OES) was also attempted to quantitatively determine the amount of nanoparticle deposited on wires in nanofluid CHF experiments. Results from ICP were compared with SEM. Finally, possible mechanisms for CHF enhancement are discussed.

2 Chapter 2 – Properties of Nanofluids

2.1 Preparation of Nanofluids

Alumina (Al_2O_3) 20% by weight (w%) was purchased from Nyacol while Silica (SiO_2) Ludox TMA at 34 w% was purchased from Sigma-Aldrich. The dilutions of the nanofluid was done using the relation reported by Kim [12] in Equation 2-1.

$$f = n \frac{\frac{1-y}{y} \frac{1-x}{x} \frac{\rho_p}{\rho_w}}{1 + \frac{1-x}{x} \frac{\rho_p}{\rho_w}} \quad (2-1)$$

Here, x is the weight percent of the original nanofluid from the vendor, y is the volumetric fraction of the desired fluid, n is the amount of x w% nanofluid, f is the amount of water required for dilution, and ρ_p and ρ_w are the densities of the nanoparticle and water, respectively. The density of Alumina and Silica nanoparticles is assumed to be that of bulk Alumina (3.90 g/ml [12]) and Silica (2.22 g/ml (measured value)). Based on Equation 2-1, in order to make 100 ml of 0.1vol% Alumina, 96.39 ml of deionized water and 3.61 ml of 20 w% Alumina would be needed. Silica and Alumina nanofluids of concentration of 0.001, 0.01 and 0.1 percent by volume (vol%) were prepared for the CHF experiments.

2.2 Nanofluids Characterization

For CHF pool boiling experiments, it is important to know the properties of the fluids that can have effects on CHF. These properties include viscosity, surface tension, thermal conductivity, pH, density and heat of vaporization. The pH of nanofluids is of interest because too low pH may damage the wire before the test, which changes the initial conditions. More importantly, according to Xuan and Li [13], pH can affect the stability of the nanofluids, which is the ability of nanoparticles to remain dispersed in the fluids instead of agglomerating into larger particles of micrometer size. The micron-size particles can have a different effect on CHF compared to that of nanoparticles [6]. While this comparison between the nanofluid and fluids

with micron-size particles is an interesting topic, we are only focusing on nanofluids' effects on CHF here.

Nanoparticles are usually produced with diameter of less than 20 nm and then are dispersed into common fluids to form nanofluids using different techniques described by Choi [14]. When the nanoparticles in the fluid agglomerate to form micron-size particles, the fluid is no longer considered nanofluid because it prevents realization of the full potential of the high surface areas of nanoparticles in nanofluids [14]. In addition, micron-size particles, unlike nanoparticle, can easily settle down, and can cause abrasion and clogging in flow system [13]. Therefore, one way to determine the stability of a nanofluid is to measure its particle size and this was achieved by Dynamic Light Scattering (DLS) technique, also known as Photon Correlation Spectroscopy or Quasi-Elastic Light Scattering. The basic set up for DLS includes a source laser, a cell sample and a detector as shown in Figure 2-1.

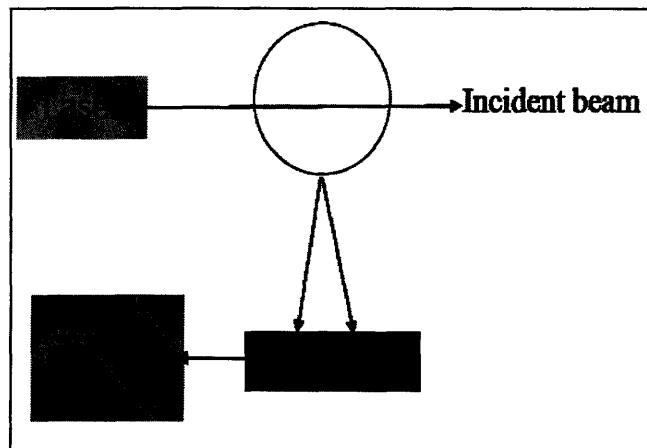


Figure 2-1: Schematic set up for DLS

DLS is a well known technique that measures the size of a particle based on its Brownian motion in the fluid. The size measured by the DLS is the hydrodynamic diameter of the particle, which is identical to the physical diameter for a spherical particle. The hydrodynamic diameter of a non-spherical particle is the diameter of a sphere that has the same translational diffusion speed as the particle does [15]. The sizes for Silica and Alumina particle in different nanofluids are listed in Table 2-1. The sampling technique used was exponential sampling, which is the most stable and reliable method to measure the size of nanoparticles dispersed in

fluids [16]. The pH values of the nanofluids are also shown in Table 2-1 since pH is one of the main factors that affect nanofluids stability. Dramatic change in pH can cause particle to agglomerate and settle out. The Alumina nanofluid is stable at pH of 4 and the Silica one is stable for a range of pH between 4 and 7, according to the vendors.

Table 2-1: Size and pH of nanoparticle in Silica and Alumina nanofluids.

Alumina nanofluids	pH (± 0.15)	Particle size (nm)	Silica Nanofluids	pH (± 0.15)	Particle size (nm)
0.001 vol%	5.07	46.9	0.001 vol%	5.97	50.3
0.01 vol%	4.61	45.2	0.01 vol%	6.91	34.4
0.1 vol%	4.25	42.2	0.1 vol%	7.64	32.9
20 w%	4.04	N/A	34 w%	7.37	N/A
Specification[17] for 20w%	4.0	50 nm	Specification for 34w%[18][19]	4.0 to 7.0	11nm

From Table 2-1, all the nanofluids used for the CHF experiment are stable since all the particles' sizes measured by DLS have diameter less than 100nm, the maximum size for a particle to be considered nano. The samples for DLS were taken from the originally diluted nanofluids. The fluids used in the CHF experiments were also taken from this large stock of prepared ones. Since these measurements were done after CHF experiments, and these fluids only had nanoparticles, the ones used in CHF experiments were still stable nanofluids. This is because particles agglomerate and settle with time in unstable nanofluids. In addition, the pH values of the dilutions did not change dramatically from those of the purchased nanofluids. All the pH values measured by a digital pH meter were checked with pH paper indicator. The measured pH values all agreed with pH paper and were at expected values except for 0.1v% Silica, which has a pH value of 7.64. This is a little bit higher than the measured value for 34w% Silica. However, the difference in pH of 0.27 is within the measurement uncertainty. More importantly, the stability of the fluids still meets specifications in defining a nanofluid.

Surface tensions of nanofluids were measured using a Sigma 703 all-around tensiometer by Wilhemy plate method from KSV Instruments [20]. The thermal conductivity of nanofluids was measured using a KD2 Thermal Properties Analyzers from Decagon Devices [21].

Finally, the kinematics viscosity was measured using a Cannon-Fenske Opaque Capillary Viscometer [22]. These properties were compared to those of water for they can have some effects on CHF. The ideal case is when these properties of nanofluids are similar to those of water. In this case any effect on CHF would be directly due to the presence of the nanoparticles, not the indirect effects due to change in fluid properties with nanoparticle present. Table 2-2 and Table 2-3 list the properties of the Alumina and Silica nanofluids used in CHF experiments.

Table 2-2: Kinematic viscosity, thermal conductivity, and surface tension of Alumina nanofluids and Water. All values, including those of water, are measured three to five times to check for consistency. The uncertainty presented is the standard error.

Fluids	Thermal Conductivity (W/m.°C) at 25 °C	Kinematic Viscosity (mm ² /s) at 40 °C	Surface Tension (mN/m) at 25 °C
Water	0.60 ± 0.0067	0.6577 ± 0.0046	67.7 ± 1.2
0.001 vol% Alumina	0.61 ± 0.0067	0.6640 ± 0.0003	67.0 ± 0.2
0.01 vol% Alumina	0.62 ± 0.0110	0.6681 ± 0.0013	47.6 ± 1.1
0.1 vol% Alumina	0.58 ± 0.0133	0.6894 ± 0.0003	40.9 ± 0.3

Table 2-3: Kinematic viscosity, thermal Conductivity, and surface tension of silica nanofluids and water. All values, except for viscosity of water, are measured three to five times to check for consistency. The uncertainty presented is the standard error.

Fluid	Thermal Conductivity (W/m.°C) 25 °C	Kinematic Viscosity (mm ² /s) at 25 °C	Surface Tension (mN/m) at 25 °C
Water	0.60 ± 0.0067	0.8900*	67.7 ± 1.20
0.001 vol% Silica	0.61 ± 0.0058	0.8846 ± 0.0027	72.1 ± 0.08
0.01 vol% Silica	0.60 ± 0.0033	0.8857 ± 0.0049	72.4 ± 0.06
0.1 vol% Silica	0.60 ± 0.0100	0.8929 ± 0.0011	72.2 ± 0.07

* Reference value from CRC of Chemistry and Physics[23]

The thermal conductivity of the Silica and Alumina nanofluids at all three volume concentrations are found to be close to the measured value of water. Notice that all thermal conductivity measurements were done at room temperature of 25 °C, and the value measured for water is 0.60 W/m-K, which agrees with value reported in CRC Hand Book of Chemistry and Physics [23]. This verifies the operation of the KD2 probe and that the measurements are valid. The viscosities of the Alumina nanofluids are very similar to that of water. However, the surface tensions of 0.1v% and 0.01v% of Alumina are significantly lower than that of water and

0.001v%. This suggests that there could be some surfactants present in the original 20w% Alumina nanofluids. However, we currently have not done enough characterization to confirm such hypothesis. The effects of lower surface tension of 0.01% and 0.1v% Alumina on CHF will be discussed in details in later chapter.

For Silica, the surface tensions of all volume concentration are around the value of water, which means that no significant amount of surfactants are present in the concentrated 34 w% Silica. Other properties of Silica nanofluids are also similar to those of water and this confirms that the presence of the nanoparticles at low volume concentration (≤ 0.1 vol%) does not affect the thermo-physical properties of a fluid.

Other properties that can have an influence on CHF are the density of liquid and vapor, and the latent heat of vaporization. The density of nanofluids can be estimated as

$$\rho_f = \frac{y * \rho_{particle} * v + \rho_w * (1-x) * v}{v} = y * \rho_{particle} + \rho_w * (1-y) \quad (2-2)$$

where y is the volumetric fraction of the nanoparticle, v is the total volume. For 0.1 vol% Alumina and Silica, the densities are 1.029 g/cm^3 and 1.012 g/cm^3 , respectively. Both are similar to water density of 1.00 g/cm^3 . The density of the nanofluid vapor is calculated, assuming nanoparticles are as volatile as water molecules are, according to Equation 2-3 [11]

$$\rho_{g-nano} = \rho_g \frac{\rho_{particle} y + \rho_w (1-y)}{\rho_g y + \rho_w (1-y)} \quad (2-3)$$

where ρ_g is the density of water vapor, ρ_w is the density of water and y is still the volumetric fraction. This gives 0.0005995 g/cm^3 and 0.0006005 g/cm^3 for vapor of 0.1 vol% Silica and Alumina, respectively, which is less than 1% different from density of water vapor. The latent heat of vaporization of nanofluids is not expected to change much compared to that of water because of low particle loading. This latent heat of vaporization can be measured in future work using a calorimeter.

Another interesting way to characterize the nanofluids is to use X-ray Diffraction Spectroscopy (XRD) because this allows one to identify the chemical composition and phase of nanoparticle in the fluid. In addition, the size of the crystal can be measured by XRD. Preliminary XRD was done for Alumina nanofluid and the spectrum is shown in Figure 2-2.

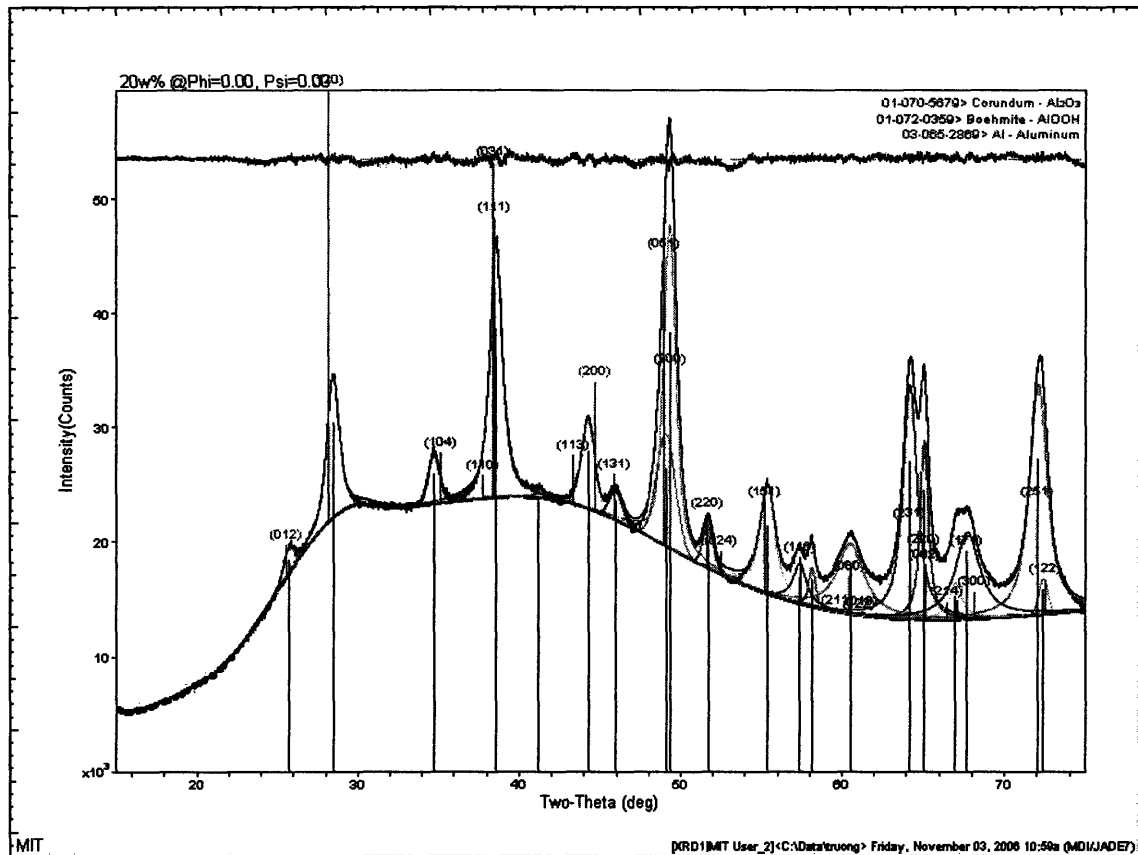


Figure 2-2: XRD spectrum of 20 w% Alumina nanofluids. Al, Corundum (Al_2O_3) and Boehmite (Al(OH)_3) are detected.

While the spectrum is only preliminary result, it already tells that the nanoparticle can be of three different compositions: pure Aluminum, Corundum (Al_2O_3) and Boehmite (Al(OH)_3). XRD spectrum on the heater after the CHF test would help to see whether there was particle deposition and its composition. The size of the crystal ranges from eight to 20 nm, and since a particle can be made of several crystals, the particle size has to be at least equal to or greater than the crystal. This confirms that the approximate 45 nm particle size measured by DLS is valid. Some other peaks cannot be identified in the spectrum and they might represent surfactants or impurities. These may have an effects on the properties of the fluids but more work is needed.

All of the above mean that any effect on CHF is not due to the change in properties of the liquid; rather, the change in CHF (if there is any) is due to other possible mechanisms that includes the present of the nanoparticles. Overall, one can say that the properties of the nanofluids used in CHF experiments are not significantly different from that of deionized water with the exception of surface tension of alumina nanofluids (0.01 and 0.1 vol%). CHF enhancement, if there is any, is not due to change in properties of the fluids but rather due to present of nanoparticles in the fluid.

3 Chapter 3 – Critical Heat Flux Mechanisms

CHF phenomenon has been studied over the past century. Nukiyama [24] was the first to study pool boiling CHF using a heated wire and the author proposed the well-known boiling curve [25], whose typical characteristics are shown in Figure 3-1. The dotted arrows represent the path of the boiling curve where it goes from CHF straight to film boiling. This is due to power-controlled heating. The main region of interest in a boiling curve is the nucleate boiling for it has high heat transfer capability and its maximum is known as CHF.

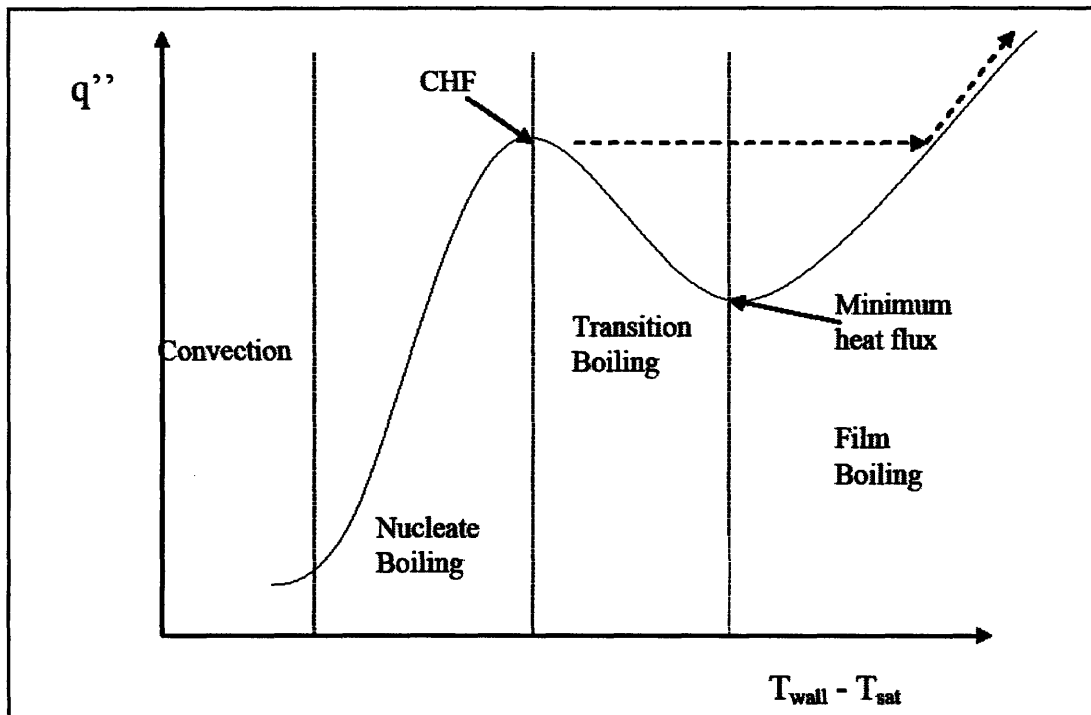


Figure 3-1: Typical boiling curve

CHF can be thought as the point where the nucleate boiling goes into film boiling, where the heater is covered with a layer of vapor film, whose heat transfer coefficient is much lower than that in nucleate boiling. Many mechanisms for CHF phenomenon have been proposed and some of the major model includes hydrodynamic instability, macrolayer dryout, local dryout, and bubble interaction.

Kutateladze [26], [27] and Zuber [28] proposed CHF phenomenon occurs due to hydrodynamic instability of the vapor jet coming from the heater. The velocity of the bubbles in the

column increases as the heat flux increases. At a critical velocity, the vapor jets experience Helmholtz instability, in which the vapor columns collapse, preventing the counter liquid flow to reach the heated surface. This Helmholtz instability occurs far above the heated surface, so this model is also known as “far field theory”. Independently, Kutateladze and Zuber came up with a correlation, known as the Zuber correlation, to predict CHF for an infinitely horizontal flat plate as shown in Equation 3-1. C is a constant, which Zuber proposed to be 0.131 while Kutateladze had C equal to 0.149.

$$q_{CHF} = C \rho_g^{1/2} h_{fg} [g(\rho_f - \rho_g)\sigma]^{\frac{1}{4}} \quad (3-1)$$

While the hydrodynamic theory concerns with the “far field effect”, the macrolayer model, originally proposed by Katto and Yokoya [29], later modified by Haramura and Katto [30], deals mainly with effect near the heater’s surface. In this model, a liquid film of some thickness, called a macrolayer, is formed and separates the heated surface under the bubble mushroom formed during nucleate boiling. The formation of the macrolayer is due to the Helmholtz instability, which causes the different regions in nucleate boiling to interfere. This layer is fed with liquid from the surround regions while the bubble grows and hovers at the heated surface. CHF occurs once this macrolayer dries out, causing the heated surface to be separated from the liquid by a vapor film, whose heat transfer coefficient deteriorates greatly compared to that of liquid film. For a horizontal cylinder heater, Haramura and Katto [30] provided the expression

$$\frac{q_{CHF}}{q_{CHF,Z}} = \left(\frac{\sqrt{3}}{R'}\right)^{\frac{1}{16}} \left[1 + \frac{1}{2(R')^2}\right]^{\frac{1}{32}} \quad (3-2)$$

where $q_{CHF,Z}$ is the CHF predicted by Zuber correlation in Equation 3-1,

and $R' = \frac{R}{\sqrt{\sigma/[g(\rho_f - \rho_g)]}}$, is the dimensionless radius. Haramura and Katto [30] assumed

that the heated surface is wettable in deriving Equation 3-2. Therefore, the effect of surface's wettability should be taken into account for non-wettable surface.

While the macrolayer dryout models concern with the evaporation of liquid film under a vapor mushroom, Zhao et al. [31] developed the microlayer model, which states that the boiling heat transfer is mainly due to the evaporation of a microlayer formed under individual bubbles. As the wall heat flux increases, the microlayer's thickness decreases, which leads to a much shorter dryout time and a higher rate of evaporation. Therefore, CHF occurs, as in the case of macrolayer, once the microlayer dries out and a vapor film is formed between the liquid and the heated surface. This microlayer model provides a continuous boiling curve as well as CHF prediction.

For small horizontal cylinders, You et al. [32] observed the local dryout mechanism for "onset of film boiling". Here, once the heat flux is high enough for a transition from natural convection to nucleate boiling, the bubble only grows in axial direction due to the ratio of the bubble's departure diameter to the wire diameter. This causes the vapor to engulf a part of the wire, subsequently makes the wire's temperature to increase due to poor heat transfer of the vapor. Therefore, the superheated liquid next to the high temperature part of the wire evaporates faster. The non-fully developed nucleation boiling has turned into film boiling, hence the term "onset of film boiling". You et al. [32] reported such mechanism were observed for wire with R' less than or equal to 0.0234. In this study, R' is 0.02429, which means the local dryout model may not apply well here.

4 Chapter 4 – CHF Experiments and Results

4.1 CHF Experiment Set Up and Procedure

4.1.1 Experimental Set Up

The set up for pool boiling CHF experiment is shown in Figure 4-1. This includes a glass rectangular test cell of outer dimensions 15.2 cm x 15.2 cm x 5.7 cm. The glass thickness is of order 0.64 cm. The glass test cell is immersed in an isothermal bath which comes with an electric heater to help maintaining the liquid in the test cell at constant temperature. The reflux condenser on top of the test cell helps to keep the pressure at atmospheric and prevents evaporation of the liquid inside the test cell, which changes the concentration of the fluid in the test cell during the experiment.

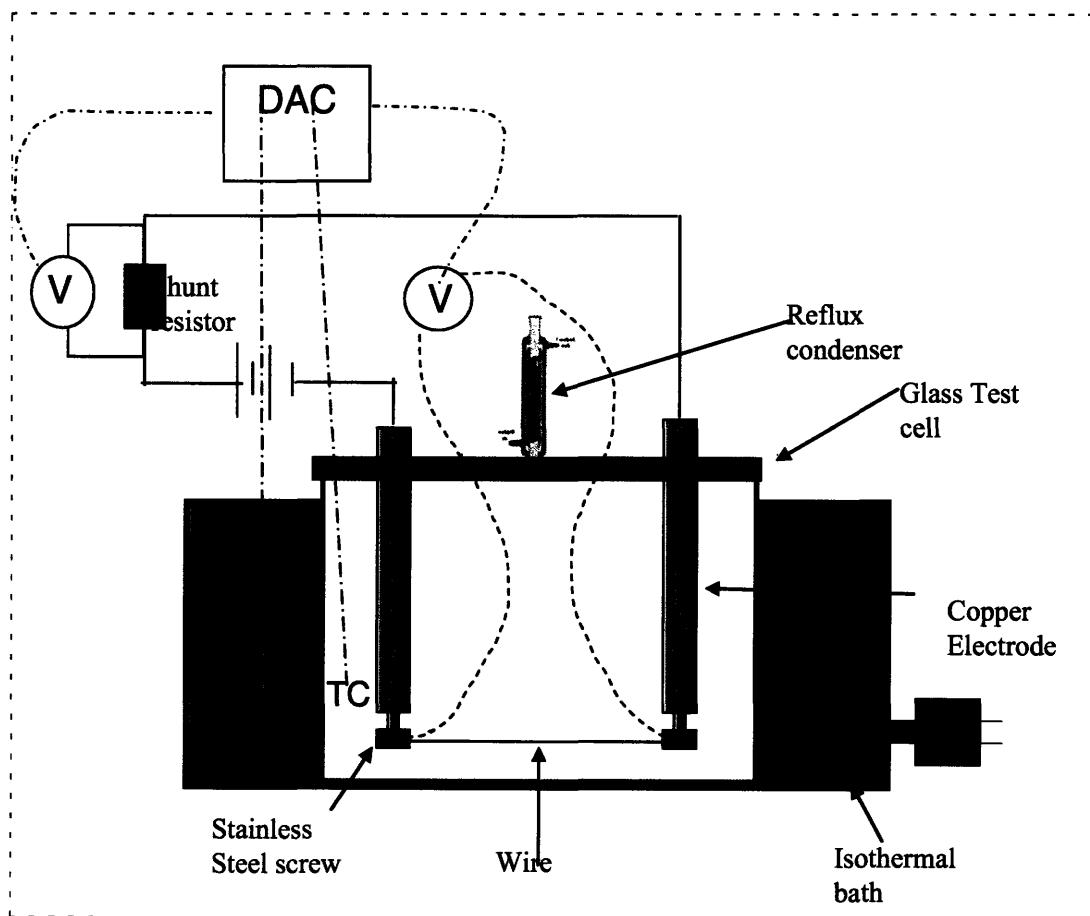


Figure 4-1 : CHF Pool Boiling Experiment Facility Set Up

The test wire is soldered to two stainless steel screws, which are tightened to the copper electrodes of 1.2 cm diameter and 15.5 cm long, and they are connected to a DC power supply. Two voltage taps are also soldered to the screws on top of the wire to measure the potential across the wire. The shunt resistor (30A by 100 mV rating), connected in series with the test wire, is used to measure the current through the wire. K-type thermocouples measure the temperatures of the fluid in the test cell and water in the isothermal bath. All data are acquired by an Agilent 34970A Data Acquisition/Switch Unit. The heat flux at any instant can be calculated as

$$q = \frac{IV}{\pi dL} \quad (4-1)$$

where I is the current, V is the voltage across the wire. d is the wire's diameter and L is the length of the wire.

4.1.2 CHF Measurement Procedure

Table 4-1 shows the experimental matrix for the pool boiling CHF measurement. For each nanofluid, CHF of three volume concentrations of 0.001, 0.01 and 0.1 percent were determined using bare stainless steel wire as heater. For water, the CHF was also measured for the case where the wire is pre-coated with Alumina or Silica nanoparticles via nucleate boiling. Procedure of these tests will be discussed shortly.

Table 4-1: CHF Experimental Matrix

Nanofluids	Volume Concentration (%) and Wire		
Water	Bare stainless steel wire and wire pre-coated with nanoparticle		
Alumina (Nyacol)	0.001v% Bare wire	0.01v% Bare wire	0.1v% Bare wire
Silica (Ludox)	0.001v% Bare wire	0.01v% Bare wire	0.1v% Bare wire

For all tests where a bare wire is used, the procedure is as follow. First a 650 ml of fluid of interest is poured into the rectangular glass test cell, which is then placed in the middle of the isothermal bath. The water in the bath is heated up to 100 °C using the electrical heater while

the liquid in cell is heated up until no further increase in temperature is observed. Temperature of fluid in test cell usually increases to approximately 96 – 97 °C. While the fluids are being heated up, the cooper electrodes, the stainless steel screws and the wire are sanded with 600-grid sand paper to and then cleaned with acetone to clean off any possible contamination (dirt, particles, etc...) on the apparatus. The prepared stainless steel 316 wire of length 9.5 cm and diameter 0.381mm is soft soldered to the two stainless steel screws, which are already tightened to the two copper electrodes. The wire is also sanded with the 600-grid sand paper and cleaned with acetone again after being soldered. This is to make sure that all wires have similar surface structure before CHF test. Voltage measurement lead wires are then soldered on top of the solder of the stainless steel wire. Once the temperature of the fluid in the cell is almost at saturation, the power is supplied to the heater wire via a DC power source. The heat flux is increased stepwise in a constant current mode until CHF occurs (the wire glows red or burns out). The profiles of current through the wire and the voltage across the wire in a typical CHF experiment are shown in Figure 4-2.

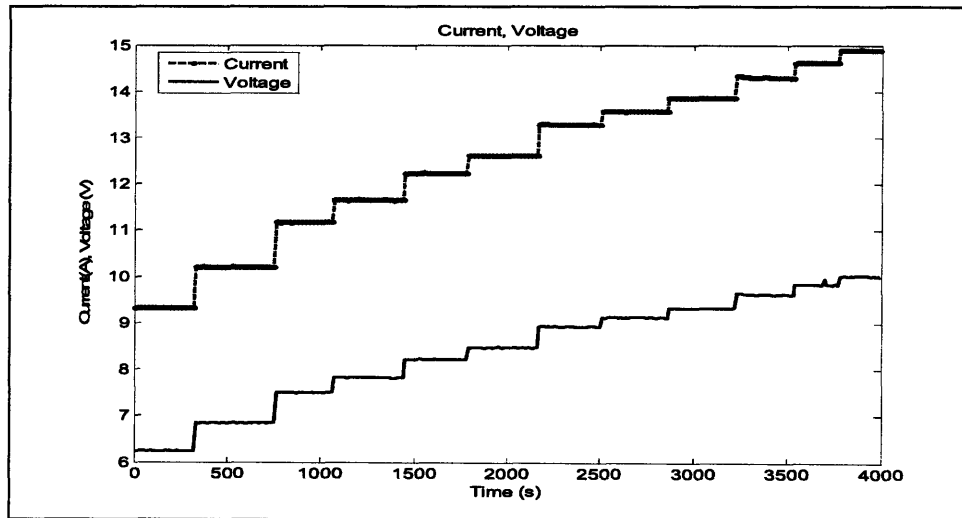


Figure 4-2: An example of current input through the stainless steel 316 wire heater for CHF measurement of Alumina nanofluid. Notice that the step size is chosen to be smaller and smaller as one approaches CHF. Once the wire glows red or burns out, CHF has just occurred. Current steps are adjusted accordingly for the liquids depending on expected CHF values.

The waiting time between each power step increase is kept at 6 minutes. This is so that the system has enough time to reach thermal equilibrium. Previous attempts where the waiting time was around two to three minutes gave scattered data. Voltage across the wire, voltage across the shunt resistor and temperatures of the liquid in the cell and of the water in the isothermal bath are measured and recorded by the DAC system. After the experiment, the stainless steel wires are stored in plastic vials in desiccators for subsequent surface characterization.

For experiments where pre-coated wire with Alumina or Silica nanoparticle was in water, the wire is first coated. This was done by boiling a bare wire in nanofluid at concentration which gave highest CHF with a bare wire. The heat flux was only raised up to 80% CHF measured and then kept at that level for the amount of time required for the bare wire to reach CHF in the nanofluid. The wires and the nanofluids were prepared identical to that of the experiments with bare wire in nanofluids. Once the wire was coated, it was transferred to a second identical glass test cell containing saturated deionized water. The power was then supplied through the wire in steps identical to the test where the bare wire was run in water until CHF was reached. Post-test characterization of the wire would help to see whether the wire had been successfully coated.

4.2 Results

4.2.1 CHF in Alumina Nanofluids

First, the CHF in deionized water was measured to be $0.83 \pm 0.059 \text{ MW/m}^2$. This is lower than the value predicted by Zuber correlation in Equation 3-1, which gives a value of 1.2 MW/m^2 for infinitely flat horizontal surface. Lienhard and Sun [33] reported a correction factor account for wire geometry with dependence on the dimensionless ra-

dius $R' = \frac{R}{\sqrt{\sigma/[g(\rho_f - \rho_g)]}}$, as shown in Equation 4-2.

$$\frac{q_{CHF}}{q_{CHF,Z}} \cong 0.89 + 2.27e^{-3.44\sqrt{R'}}, R' > 0.15 \quad (4-2)$$

Again, $q_{CHF,Z}$ is the CHF predicted by the Zuber correlation in Equation 3-1. In our experiments with saturated water, $R' = 0.02429$, which means that Equation (4-2) will not apply in predicting CHF. This is due to the fact hydrodynamic instability mechanism does not govern CHF for R' less than 0.1, according to Lienhard and Bakhru [34], for $0.01 < R' < 0.15$ is in transition regime where hydrodynamic mechanism starts to take place. In addition, the CHF results for $R' < 0.15$ is scattered, as shown in Figure 4-3.

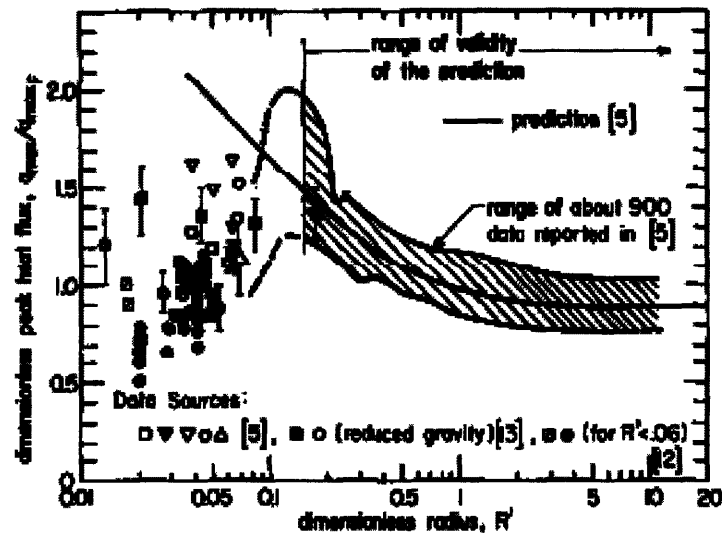


Figure 4-3: CHF Data for Different Dimensionless Radius, R' (figure taken from Lienhard, et al. [33])

Notice that for $R' < 0.06$, the ratio $\frac{q_{max}}{q_{max,Z}}$ varies from 0.5 to 1.0, which means that the CHF

values can be anywhere between 0.6 to 1.2 MW/m² for water. The CHF for water here is 0.83 MW/m², which falls right between the acceptable ranges. Therefore, 0.83 MW/m² can be used as a base CHF value for comparison with those of nanofluids.

The CHF values measured in water and in Alumina nanofluid of 0.001 to 0.1 volume percent is shown in Figure 4-4. The CHF enhancement in Alumina nanofluids is observed at all volume concentration. However, there seems to be a non-monotonic relationship between percent

enhancement and volume concentration. Indeed, 0.01 vol% Alumina gives the highest enhancement of 56.4%. Notice that pre-coated wire in water gives CHF value equal to that of bare wire in 0.01 vol% Alumina, which was used to coat the wire. This means CHF enhancement is due to the nanoparticles deposited on the wire heater's surface, not the nanoparticles suspended in the fluid. Wire surface characterization, which is discussed in the next chapter, will give further insight about this aspect.

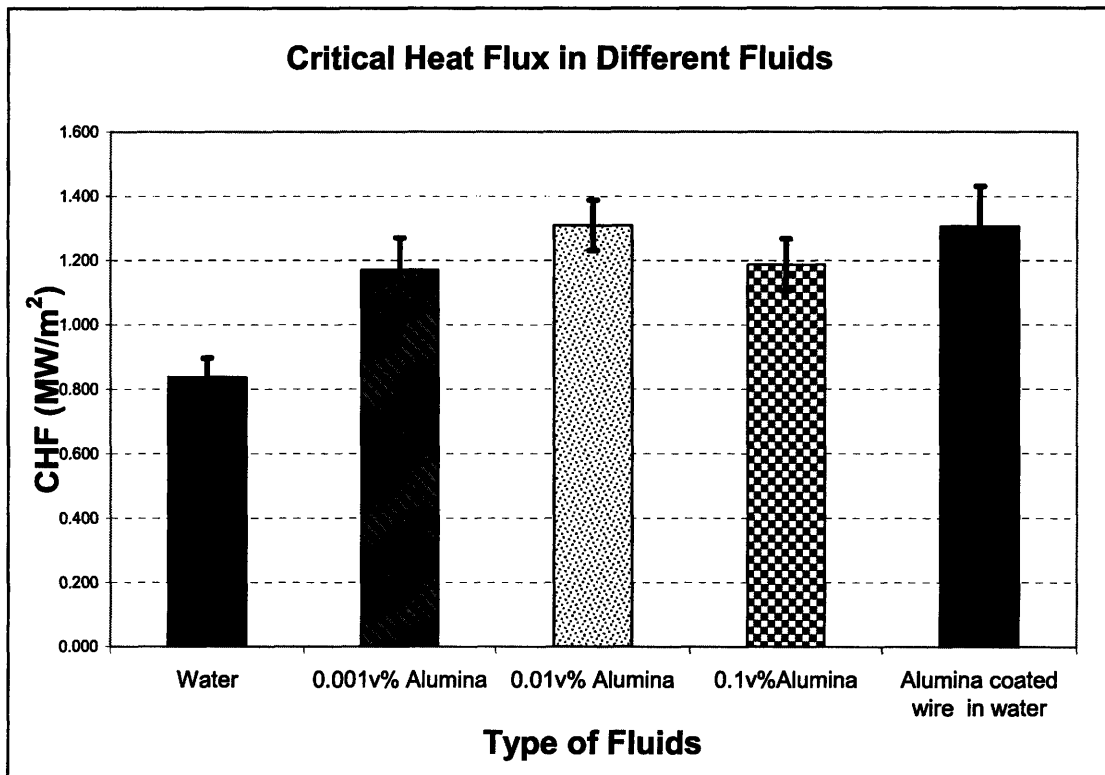


Figure 4-4: CHF values in Alumina of different volume concentration. Notice that higher volume concentration does not correspond to higher CHF enhancement. The percent of CHF enhancement are 39.7%, 56.4% and 42.0% for 0.001%, 0.01% and 0.1% by volume Alumina, respectively. Pre-coated wires by 0.01 vol% Alumina in water give enhancement in CHF similar to that of bare wire in 0.01 vol% Alumina. Values reported are the average of three experiments and the error bar represents uncertainty in measurement and from standard error. The total uncertainty in these experiments is maximum 10%.

Another interesting aspect of heat transfer is the boiling curve, which plots the heat flux as a function of the difference in temperature between the wire and the liquid. The boiling curves give information about the heat transfer coefficient. The temperature of all nanofluids at satu-

ration is 100 °C at atmospheric pressure [35]. The temperature of the wire is deduced from the wire's electrical resistance by the following relationship [36]

$$r(T) = r(T_0) * (1 + \alpha(T - T_0)) \quad (4-3)$$

where T_0 is the initial temperature of the wire, which is approximately 100 °C when power is first supplied to wire. r is the resistance and α is the temperature coefficient of resistance of stainless steel, which is $0.000774 \text{ } \Omega/(\Omega\text{-}^\circ\text{C})^1$. We are assuming the value of α is constant in the temperature range from 100 to 150 °C. The resistance of the wire is obtained from the voltage measured across the wire and the current is determined from the shunt resistor.

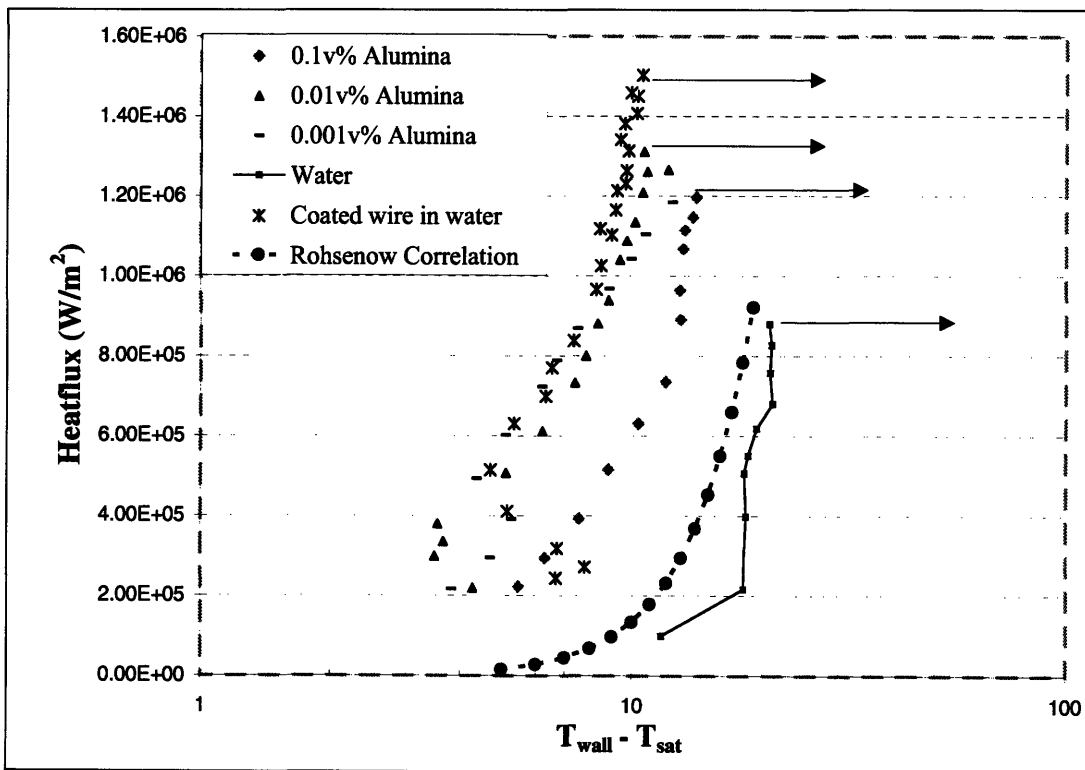


Figure 4-5: Boiling curves for Alumina nanofluids of different volume concentration and of water with bare stainless steel wire and pre-coated wire. Notice all the curves for nanofluid are shifted to the left of that of water.

The boiling curve for water closely matches the Rohsenow's correlation [37] which applies in nucleate boiling region, at the higher superheated temperature. For example, for ΔT of 18°C,

¹ Value deduced from graph in ASME handbook, code 1307, p. 19.

Rohsenow gives 0.78 MW/m^2 heat flux while the measured value is 0.50 MW/m^2 , which is within 36%. For ΔT of 20°C , the heat fluxes are 0.75 and 1.02 MW/m^2 for measured value and Rohsenow, respectively, which is 25% different. The ΔT for water should increase with increasing heat flux but that is not the case here. This is due to the limited resolution of the DAC system which cannot detect too small changes in the stainless steel wire's resistance. Hence, the ΔT sometimes scatters. With Rohsenow correlation's typical error of 100% in predicting heat flux, 25% error in ΔT [27], and the fluctuation in the deducing ΔT , the experimental technique and data are considered valid. Notice here that all the boiling curves in nanofluids or with nanoparticle coated in wire are shifted to the left compared to that of water. This means that the heat transfer coefficients, h , of nanofluids are higher than that of water since

$$Q = h_c A(T_{wall} - T_s) \Rightarrow h = \frac{Q}{A(T_{wall} - T_s)} \quad (4-4)$$

and this is shown in Figure 4-6.

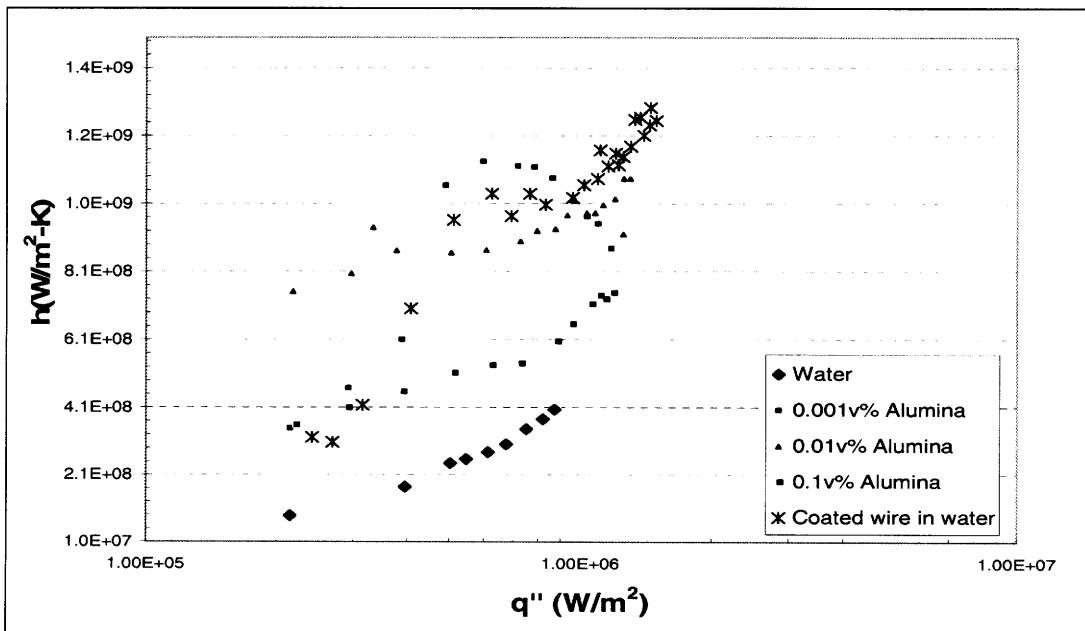


Figure 4-6: Heat transfer coefficient as a function of heat flux. The general trend here is that the heat transfer coefficients increase with higher heat flux. Heat transfer coefficient of water is less than that of nanofluids.

The enhancement in heat transfer coefficient as well as CHF in Alumina nanofluids is significant because this will allow a larger amount of heat from the heater surface to be transferred more effectively. This, combining with a higher CHF, means that power density of a system can be increased and a larger safety margin can be achieved.

4.2.2 CHF in Silica Ludox TMA Nanofluids

For Silica nanofluids, CHF of all three volume concentrations of 0.001%, 0.01% and 0.1% were measured. The case with wire coated with Silica (by boiling in 0.1 vol% nanofluid) in water was also run to see if the same phenomenon as in Alumina nanofluids occurs. The CHF of Silica nanofluids are shown in Figure 4-7.

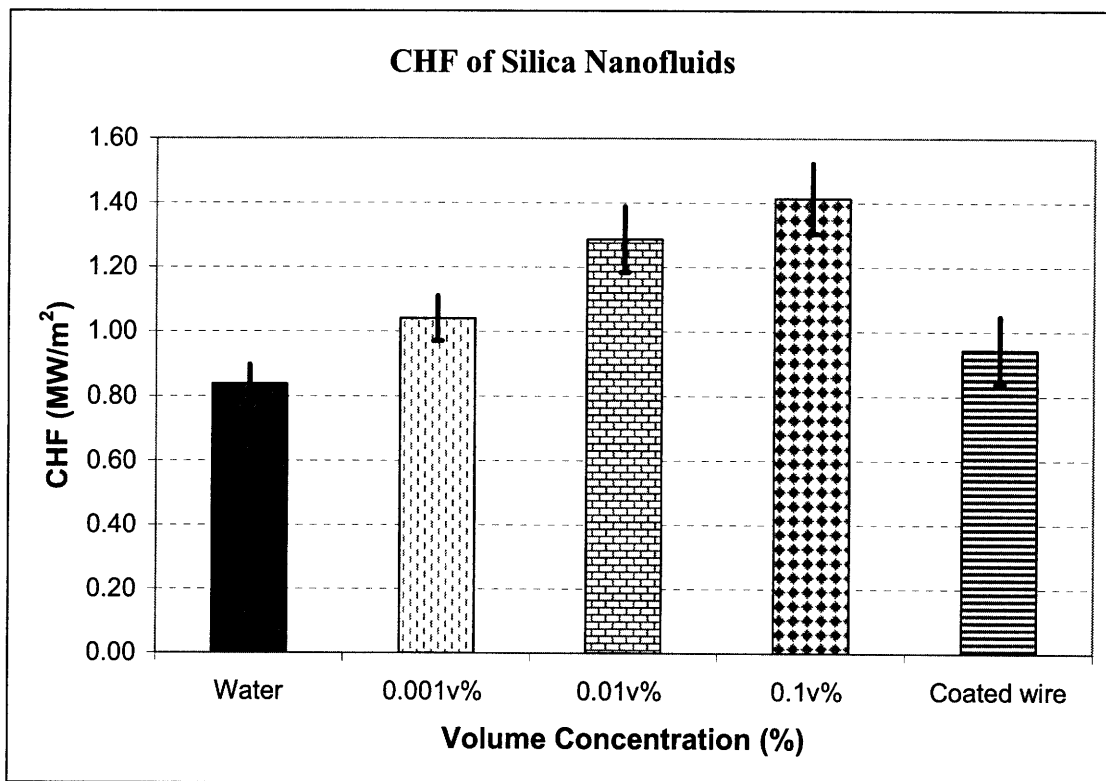


Figure 4-7: CHF in Silica Nanofluids. There is an enhancement in CHF for every volume concentration and the magnitude increases with volume concentration. The coated wire in 0.1 vol% Silica only had very little CHF enhancement in water. The error bar combines both measurement error and standard error.

Similar to Alumina, Silica nanofluids have CHF enhancement even at 0.001% volume. However, Silica nanofluid has a monotonic relationship between CHF enhancement and concentration. Also, Silica enhances CHF up to 68% while Alumina has only 56% higher than CHF in

water. The results here confirm once again the ability of nanofluid to enhance CHF. However, the case where the wire was pre-coated with Silica and then run in water did not seem to give much of an enhancement. This may mean that either the coating on the wire was not as successful or that the coating layer fell off. The SEM images of the wires, which will be shown in the next chapter, will give more insight. The boiling curves for Silica nanofluids are compared with water in and the heat transfer coefficients as function of heat flux is shown in Figure 4-8 Figure 4-9.

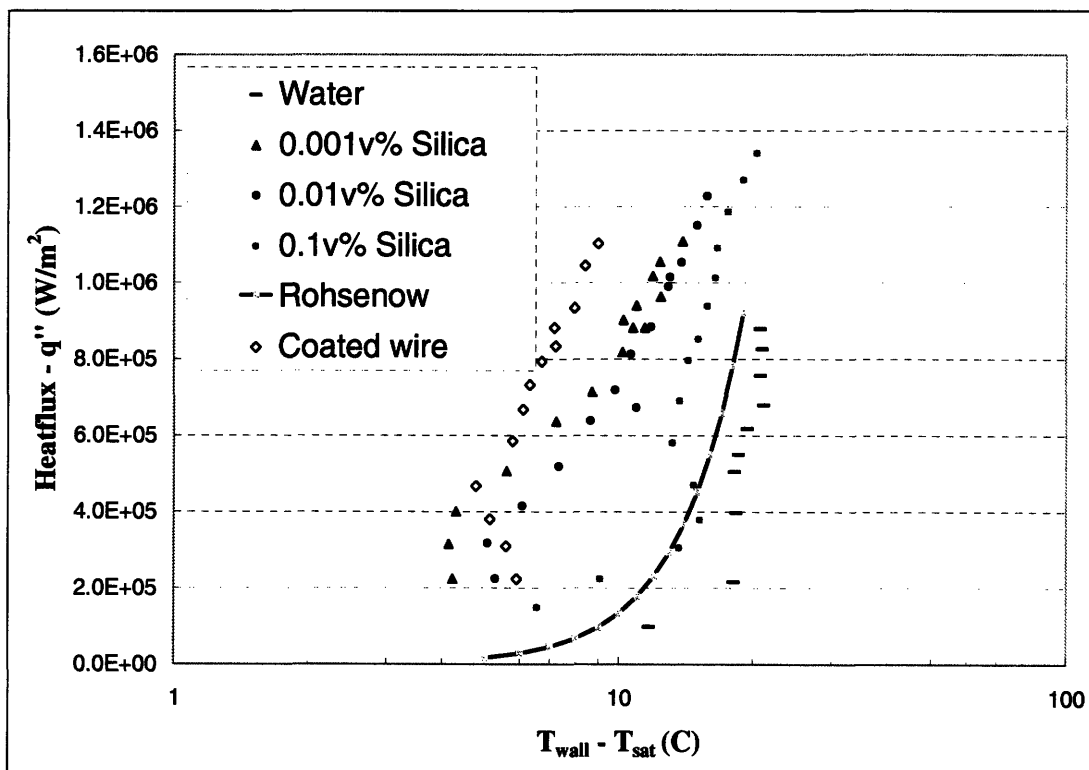


Figure 4-8: Boiling curves in Silica Nanofluids compared to that of water and the Rohsenow correlation. The curves for Silica nanofluids are shifted to the left of the curve for water. The ΔT for wire in Silica is higher than that of wires in Alumina nanofluids.

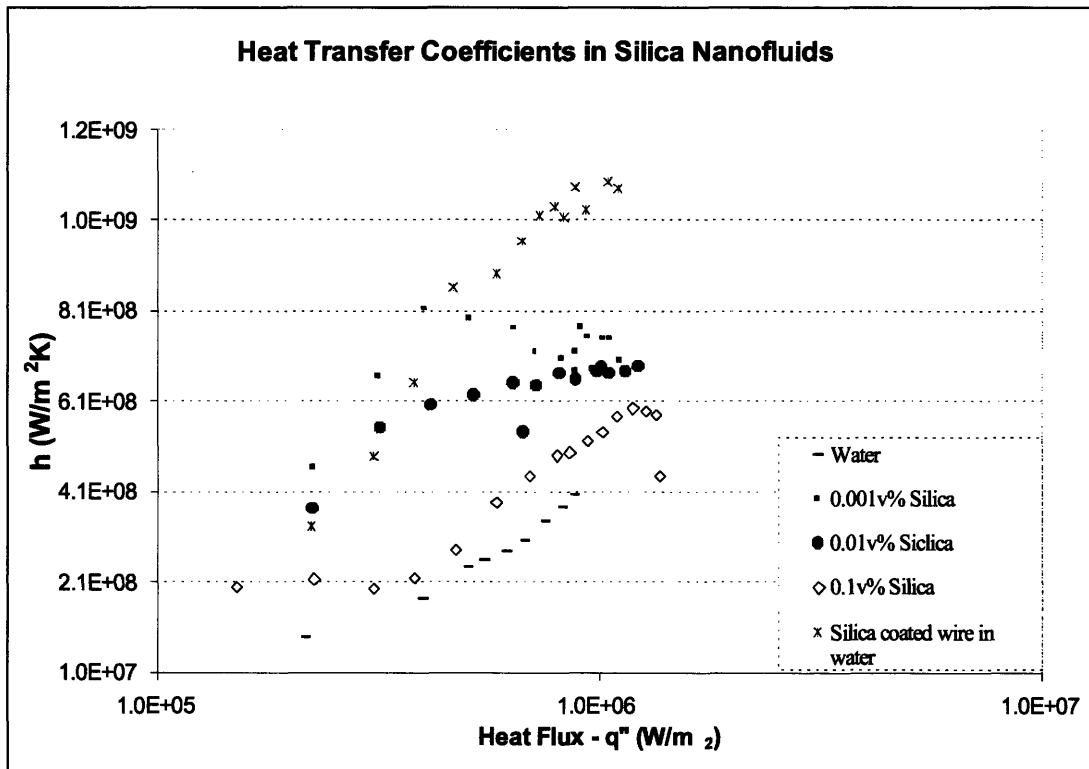


Figure 4-9: Heat transfer coefficients in Silica nanofluids

Again, similar to Alumina, the boiling curves in Silica nanofluids also shifted to the left of the boiling curve in water. This means that the heat transfer coefficient of Silica nanofluid is also higher than that of water in nucleate boiling. Notice that the coated wire, even though it did not provide a CHF enhancement, still has higher heat transfer coefficient.

5 Chapter 5 – Characterization of Heater's Surface

5.1 SEM Characterization

5.1.1 Wires in Alumina Nanofluids

Wires in CHF experiment were characterized using SEM to see the change in surface morphology. Figure 5-1 compares the surfaces of the wires subjected to Alumina nanofluids of different concentration and water.

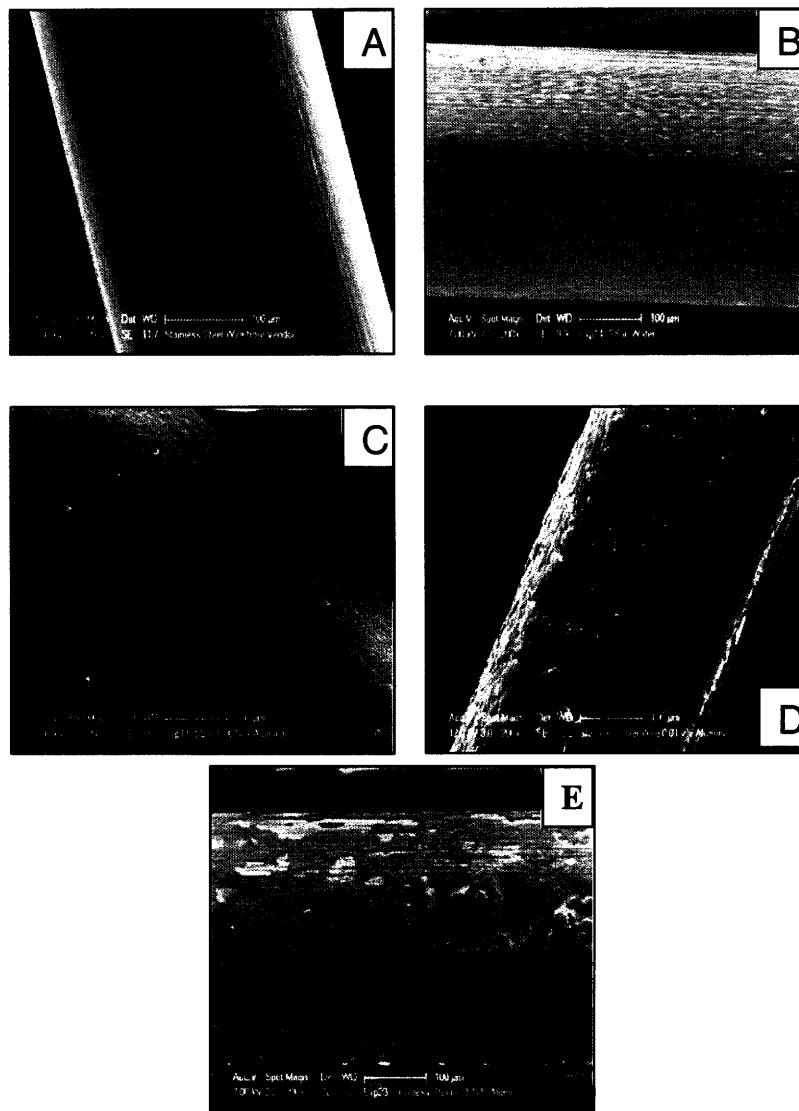


Figure 5-1: SEM image of stainless steel wires in after CHF experiments. A: Bare wire (after sanded with 600 grid sand paper); B: Wire boiled in de-ionized water; C: Wire boiled in 0.001 vol% Alumina; D: Wire boiled in 0.01 vol% Alumina; E: Wire in 0.1 vol% Alumina. There are coatings of Alumina nanoparticle on wires in nanofluids while original wire (A) and wire in water (B) have no coating of nanoparticles.

The bare wire from vendor (Figure 5-1 A) and the wire in water (Figure 5-1 B) look much smoother compared to the wires in Alumina nanofluids. This verifies the deposition of nanoparticles on the wires which were run in nanofluids. Notice that the coating of the wire in 0.001 vol% Alumina is more uniform compared to that on wire in 0.01 vol% or 0.1 vol% Alumina. A possible explanation for this is that the coating layer reaches saturation at some thickness. For 0.001 vol% the layer is fairly uniform, possibly due to the fact that there were not enough particles deposited to reach the saturated thickness. However, for 0.01 vol% and 0.1 vol% Alumina nanofluids, a lot more particles are available to deposit, which eventually build up to the saturated thickness. Any extra particle tries to deposit on the surface then may or may not stick, resulting in a flaky pattern as in 0.01 vol% or fragmented one as in 0.1v% Alumina. Figure 5-2 compares the surfaces structure of the wires subjected to the same conditions in CHF experiment. The coating layers are observed to be similar for two wires in the same conditions. For example, Figure 5-2 A and B are images of two wires in 0.1v% Alumina and they both have a segmented layer pattern. The flaky pattern is also seen in Figure 5-2 C and D, which are images of wire in 0.01v% Alumina. This confirms that the mechanism in which the nanoparticles deposit on the wire's surface stays the same in experiments using the same nanofluids. Figure E and F in Figure 5-2 are of wires boiled in 0.001 vol% Alumina. They have similar coating pattern but E seems to have some fragments get peeled off. This probably occurred during handling of the wire, where pieces of the deposited particles fell off, but the layer still seems smooth as in Figure F.

It is also of interest to see when the nanoparticles deposits on the wire. Therefore, the experiments where the wire is pre-coated by pool boiling in 0.01v% Alumina up to 80% CHF were performed. As already mentioned, these coated wires in water gave similar CHF enhancement compared to bare wire in 0.01v% Alumina. In addition, the wire's surface structures of these pre-coated wires are similar to that of the wires in 0.01v% Alumina, as shown in

Figure 5-3. This means that the nanoparticles deposit on the wires sometimes during nucleate boiling. The mechanism for the deposition will be discussed shortly.

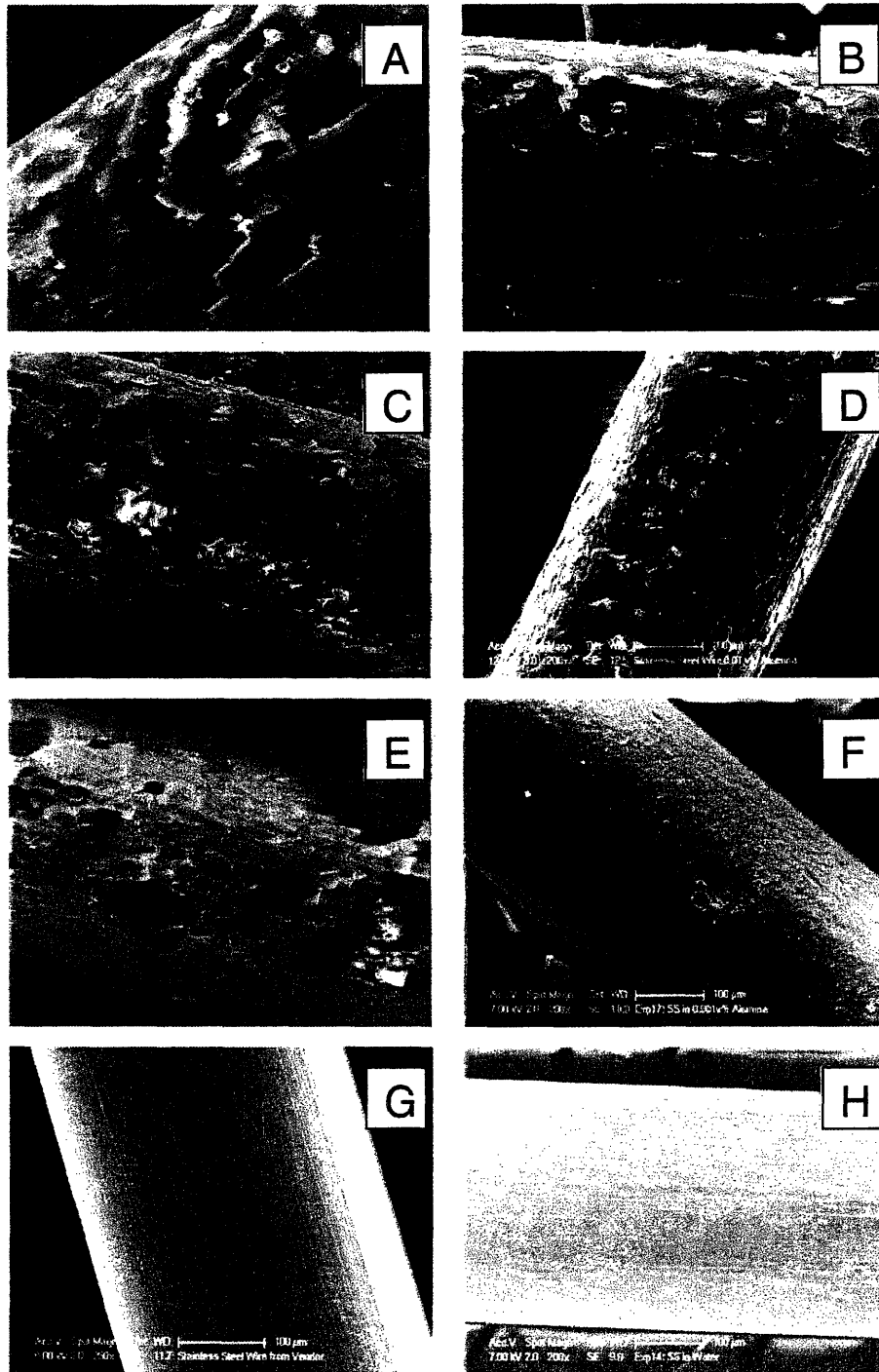


Figure 5-2: SEM images (200x magnification) of wires in Alumina nanofluids of 0.1v% (A, B), 0.01v% (C, D), 0.001v% (E, F), original wire (G) and wire boiled in water (H). The coating patterns of nanoparticle on the wire in different volume concentrations are different but two wires in the same volume concentration share many similar coating structures.

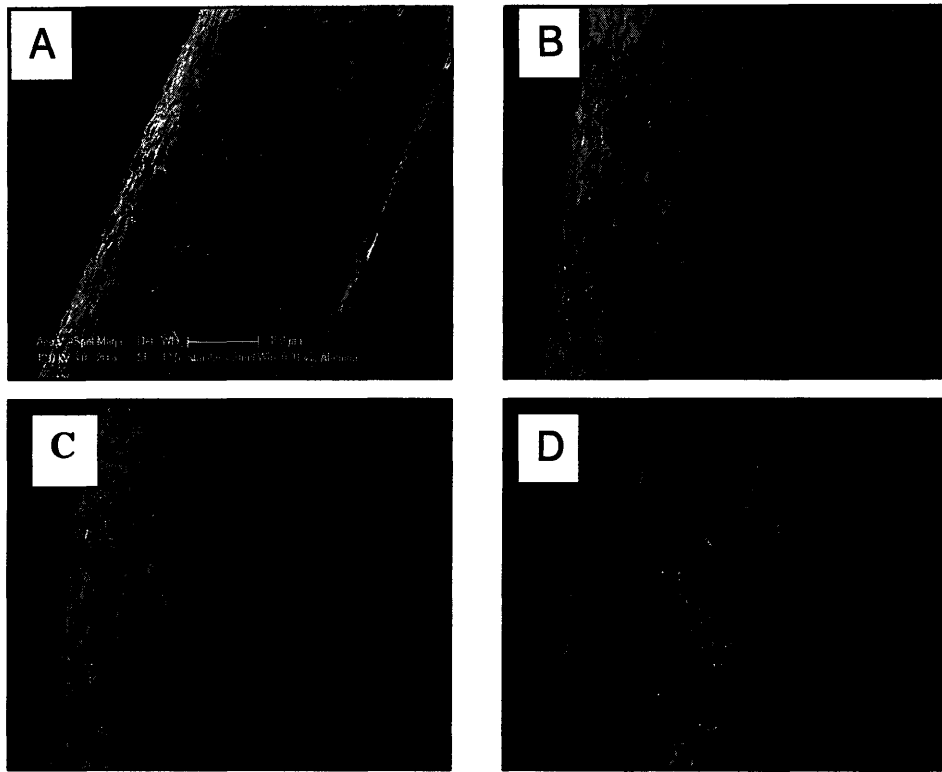


Figure 5-3: Comparison between SEM images (200x magnification) of wire in 0.01v% Alumina (A) and pre-coated wires in de-ionized water (B, C, D). The coating patterns of all wires have similar structures.

To verify further that the nanoparticles deposited on the wire are actually Alumina (Al_2O_3), Energy Dispersive Spectroscopy (EDS) was used to identify the elemental composition of the coating layers observed on the wire's surface. Al and O are the two main elements identified in the coating layer while the peak for Fe corresponds to the stainless steel wire can be observed when the coating layers are not thick enough and/or not present. These results are shown in Figure 5-4.

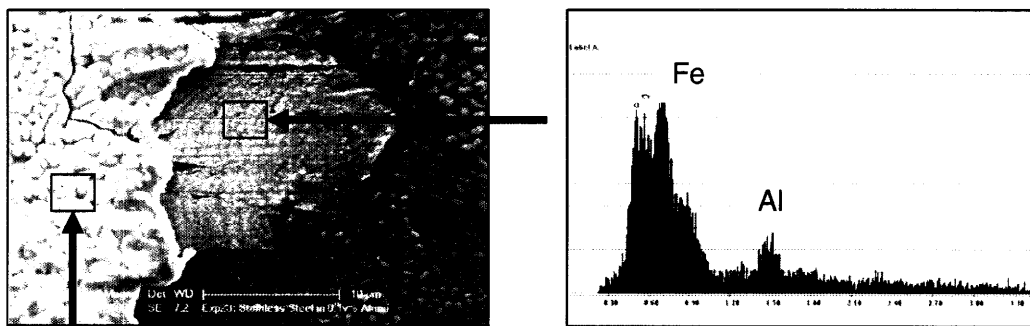


Figure 5-4a: SEM image (3500x) of stainless steel in 0.1%v Alumina with EDS spectra. The left spectrum shows only Al and O present for the region with thick coating layer while the top spectrum shows Fe can be detected when the coating layer is not as thick. Al and O are still detected at this region.

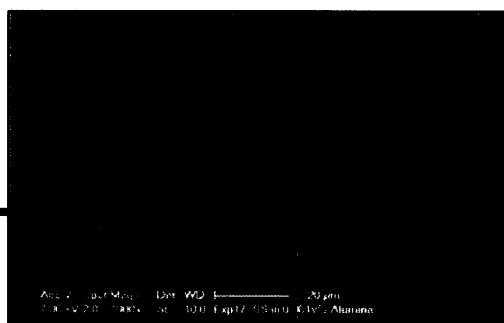
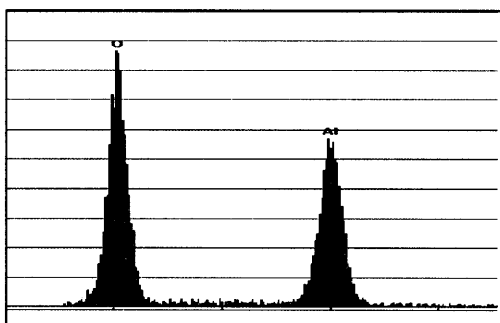
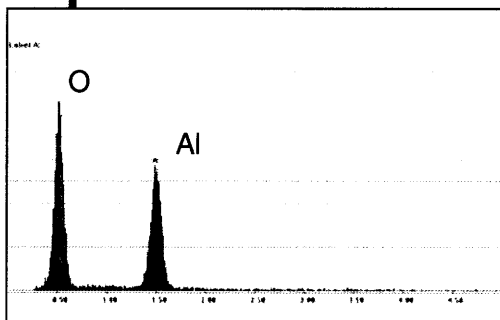
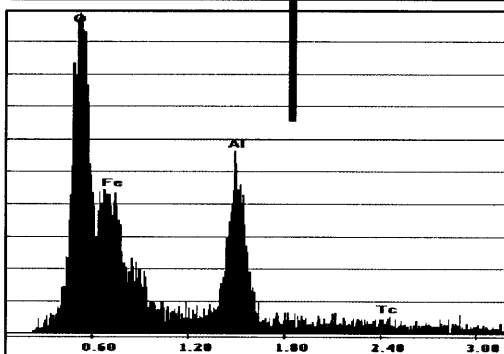


Figure 5-4b SEM image (1000x) of wire in 0.001%v Alumina with EDS spectra. The top spectrum shows only Al and O present or the region with thick coating layer while the right spectrum shows Fe can be detected when the coating layer is not too thick. Al and O are still detected at this region



It is of interest to estimate the amount of Alumina nanoparticles deposited on the wire's surface. One method is using SEM to look at a wire mounted vertically. The approximate thickness of the particles then can be measured using measurement tool in SEM software. Figure 5-5 shows the set up for such measurement.

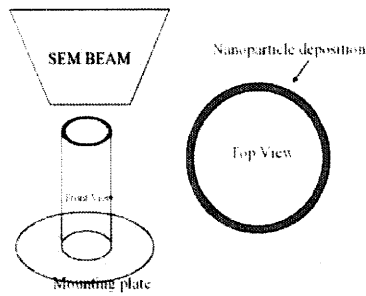


Figure 5-5: Wire is mounted vertically on SEM mounting plate in order for the thickness of the nanoparticle deposition can be approximately measured.

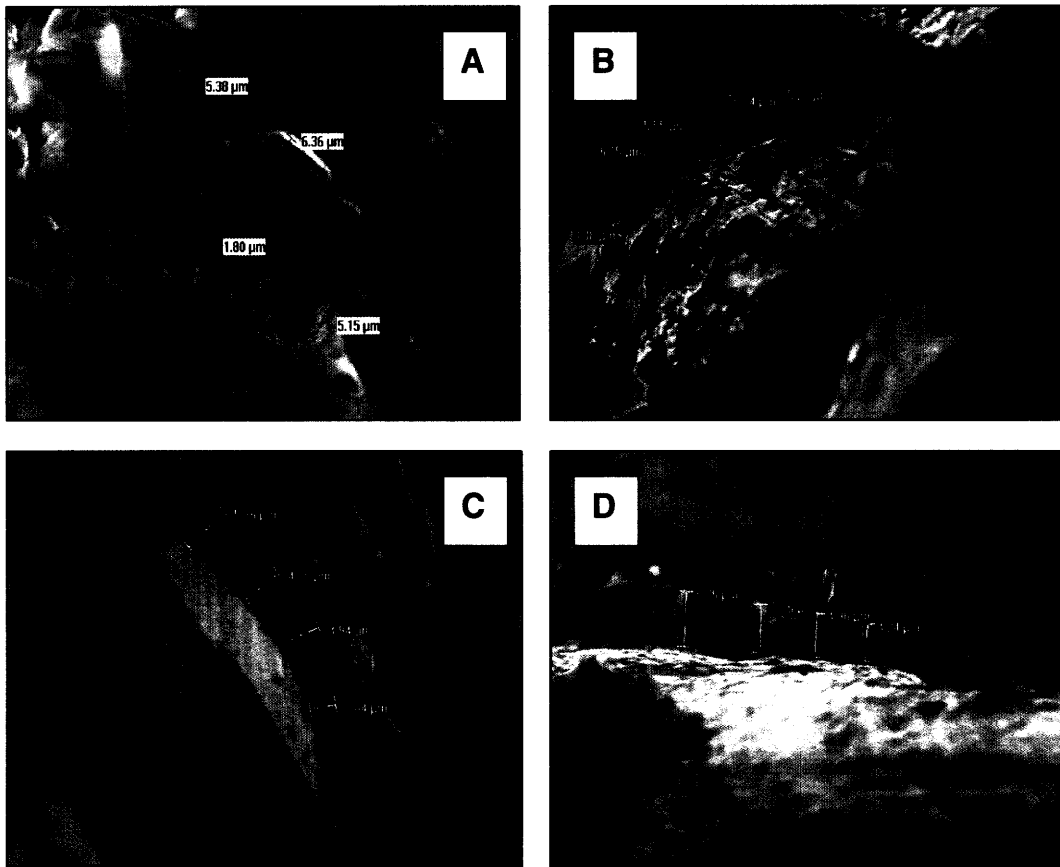


Figure 5-6: Approximate thickness of coating layer on wires in Alumina nanofluids of different concentration. A – wire was coated in 0.01v% up to 80% CHF and ran in water; B – Wire in 0.001v%; C – Wire in 0.01v%; and D – Wire in 0.1v% Alumina

Figure 5-6 shows the thickness of the coating layers on the wires in Alumina nanofluids subject to different volume concentration. Notice that the thickness ranges from three to six micrometers and the layers of different wires seem to have approximately the same thickness. However, since the bottom plane where the thickness is measured from could also be Alu-

mina, the thickness measured here can be underestimated. Therefore, it is hard to distinguish which volume concentration allow the most nanoparticles deposited. In addition, inhomogeneity of the deposited layer does not allow exact measurement either. Nevertheless, the measurement here gives insight about the amount of nanoparticles deposited.

5.1.2 Wires in Silica Nanofluids

SEM images of wires in Silica were also taken and the results are shown below in Figure 5-7, Figure 5-8, Figure 5-9, Figure 5-10.

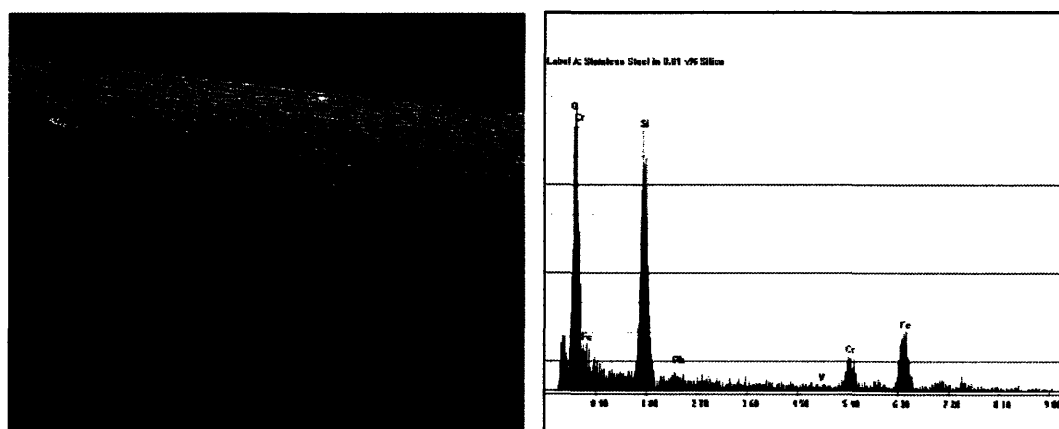


Figure 5-7: Stainless steel wire tested in 0.001vol% Silica with EDS and thickness measurement, which gives 3 to 6 micrometer of deposited particle.

In Figure 5-7, the wire has nanoparticle deposition, which seems to be fairly uniform. EDS on the whole wire shows Si and O as well as elements (Fe, Ni, Cr) making up stainless steel. This means that either the layer is not thick enough so that the x-ray can penetrate through it to reach the stainless steel or there are some spots with very little deposition. The SEM image

from vertical view verifies that there are spot without too much deposition. The thickness of the coating layer is of the order of three to six micrometers.

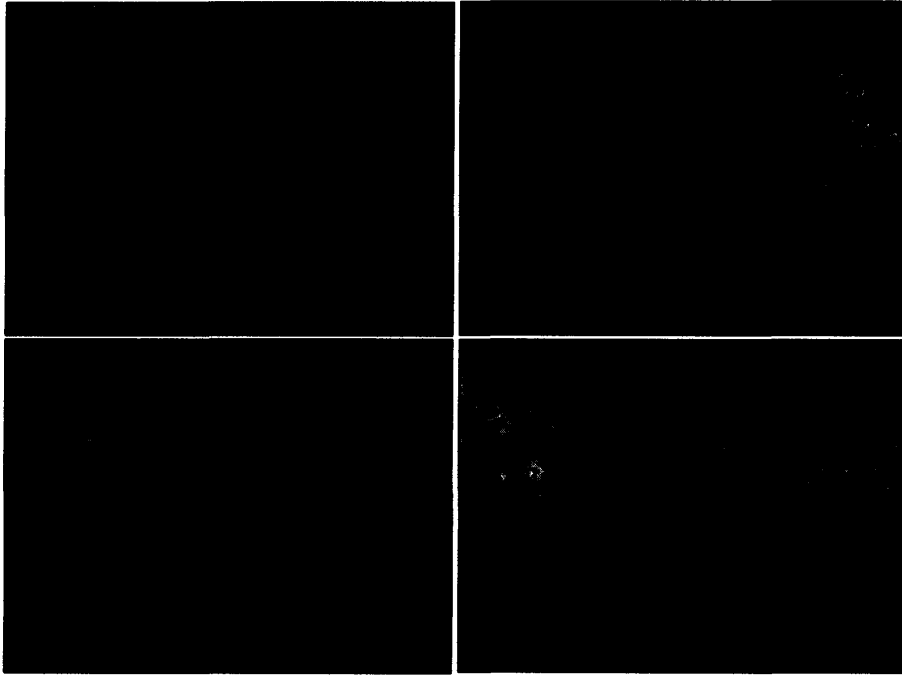


Figure 5-8: SEM of wires in 0.01 vol% Silica (left figures) and 0.1 vol% Silica (right figures).

In Figure 5-8, SEM images of two wires in 0.01 vol% Silica and two wires in 0.1 vol% Silica are shown. The wires in the same concentration seem to have similar coating pattern. The coating layers on the wire in 0.1 vol% Silica seems to be a little bit thicker than those on wires in 0.01 vol%. None of the wire seems to have any uniformity in the coating layer. There are random spots where the wire can be seen. This can mean that either the nanoparticle did not coat the wire or the deposition has fallen off, which can be seen on the top right image.

In Figure 5-9, the wire was viewed by SEM from vertical direction so that the thickness of the deposited layer can be estimated. Here, the boundary between the wire and the layer are clearly defined. The thickness of the deposited layer ranges between 8.5 to 14.8 μm . EDS spectra of two locations verify the composition of the materials. The EDS spectrum on the left was taken on the coating layer, which shows to have only Si and Oxygen as expected. The bottom EDS spectrum has peaks for the common elements found in stainless steel such as

Chromium and Iron. Some traces of Silicon are also seen on the bottom spectrum because stainless steel wire has Silicon (around 1%) as an impurity. Nevertheless, the two EDS spectra help to confirm the clear distinction between the wire and the coating layer.

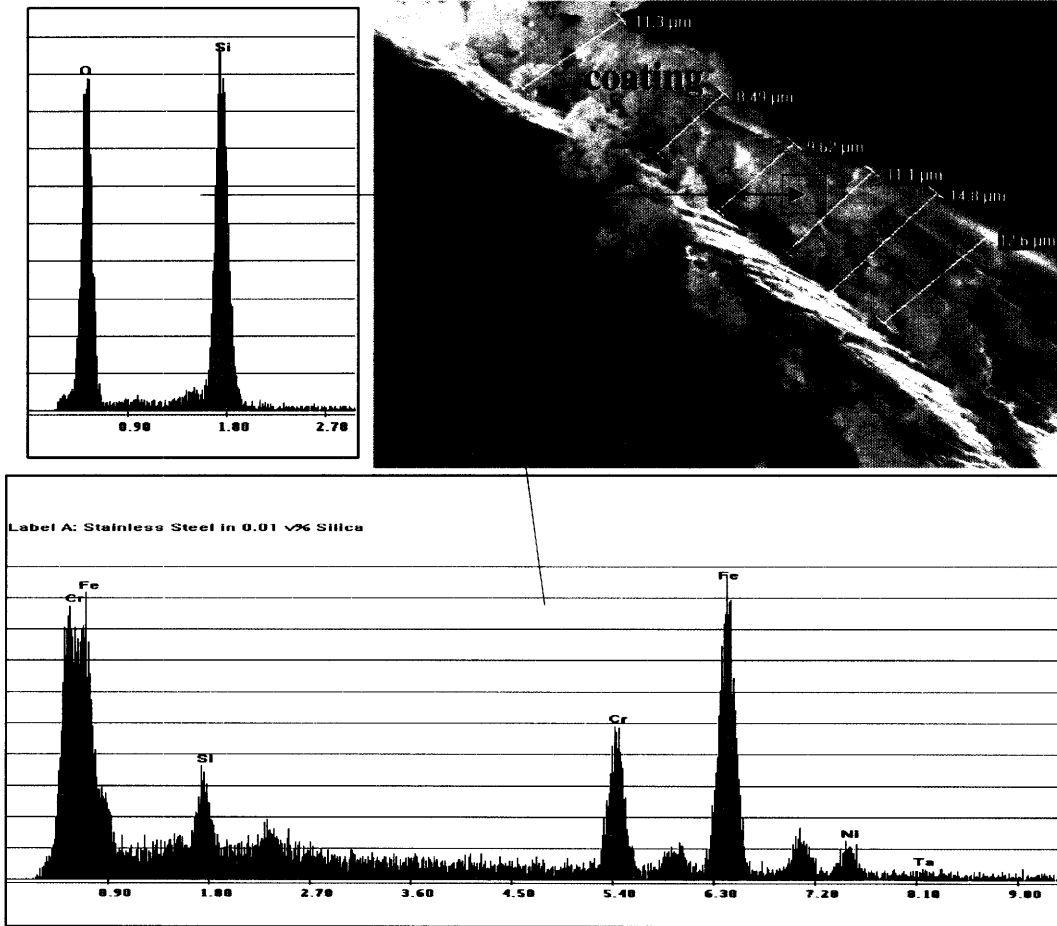


Figure 5-9: Vertical view of wire in 0.01 vol% with thickness measurement and EDS to identify elemental composition. The boundary between the wire and the deposited layer of particle is clear here.

Figure 5-10 shows the thickness estimate of the coating on the wire in 0.1 vol% Silica nanofluid CHF experiment. These four images are taken within less than 1cm-long piece of wire. Notice the differences in the approximate thickness at various locations. This means that the coating is not uniform through out the wire. All these images confirm the change in wire surface's morphology.

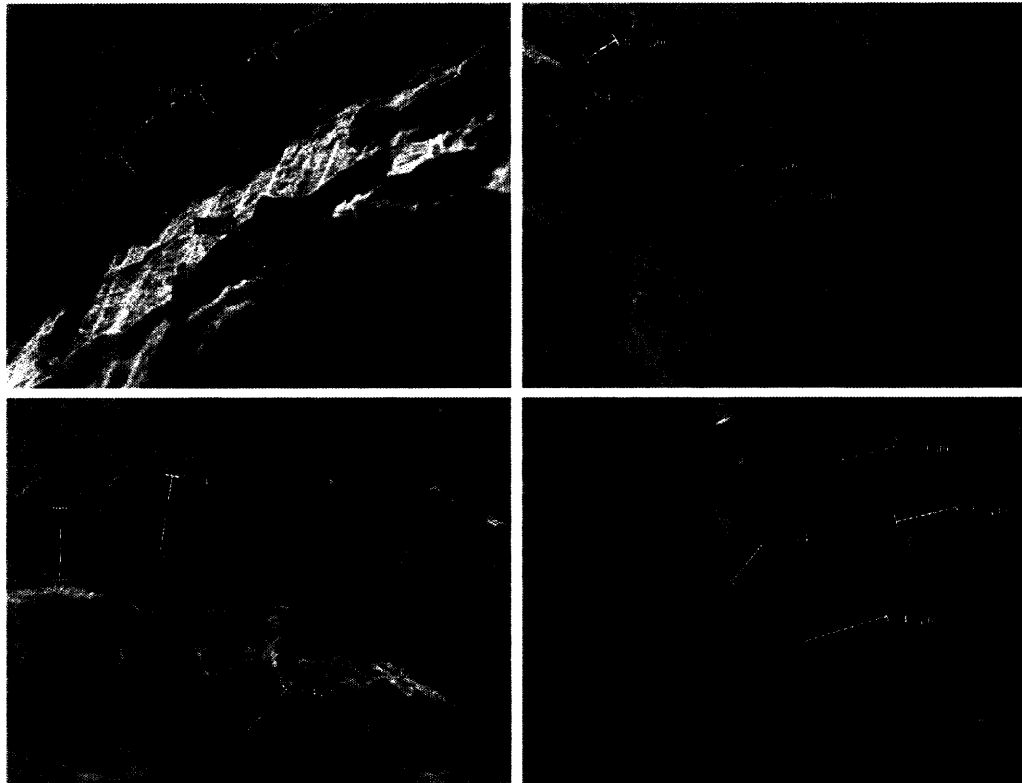


Figure 5-10: SEM of wire view from vertical at different locations. The thickness varies anywhere from a few to more than 20 micrometers over this less than 1 cm of the wire.

According to Figure 4-7, no to little CHF enhancement was observed for the case where the wire is pre-coated with Silica and then run in water and Figure 5-11 points to a possible reason. The SEM images of two wires only have sporadic spots of Silica but there are no real coating layers as when the bare wires were boiled in Silica nanofluids. The surface structure of the two wires here are more similar to the bare wire in water, and hence they have similar CHF values. While this confirms further that CHF enhancement in nanofluids is due to change in heater surface's morphology with deposition of the nanoparticles, it raises an interesting point about the differences in coating mechanism and stability of the layer deposited by Alumina and Silica nanoparticles. Apparently, Silica coating layers are not as stable as that of Alumina and this observation could be explored in future work where the physical and chemical properties of the layer and how they interact with the heaters are investigated.

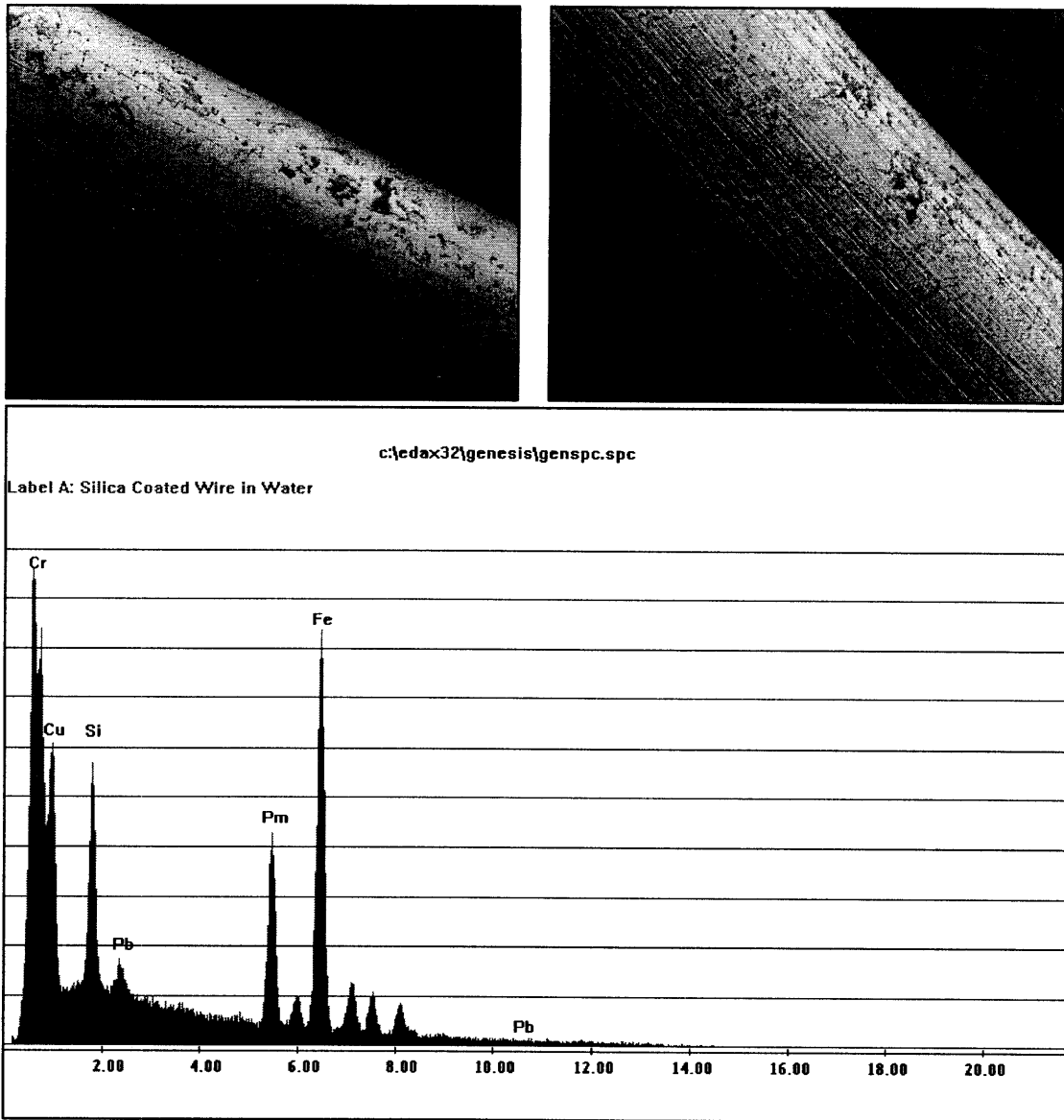


Figure 5-11: SEM images of two pre-coated (via nucleation boiling in 0.1 vol% Silica nanofluids) wires with Silica in water CHF tests. There is no coating layer; rather, there are sporadic spots of Silica on the wire. EDS spectrum on the wires does not show any present of Silica (no O detected). The peak for Silicon probably comes from the 1% Silicon in the wire. The peak for Pm probably comes from impurities.

5.2 Analyses

5.2.1 Mechanism for Particle Deposition

Figure 5-3 in previous section shows that the wires boiled in 0.01% Alumina nanofluids until 80% of CHF have similar coating compared to the wire that was in the same fluid until CHF is reached. This means that the particle deposition must have occurred during nucleate boiling. Kim et al. [11] explained that particle deposition during nucleation boiling is due to evaporation of microlayer formed under vapor bubble growing. The nanoparticles already in the water settle down on the wire during this evaporation process. This explanation does not take into account of nanoparticle diffusion but it still provides a reasonable estimation of particle deposition for short amount of time (6 minutes) on flat heaters during nucleation boiling. However, the CHF experiments here take more than an hour each and the geometry of the heater is a small cylindrical wire. The mechanism provided by Kim et al. [11] does not explain saturation of deposition, which is observed on wire heaters.

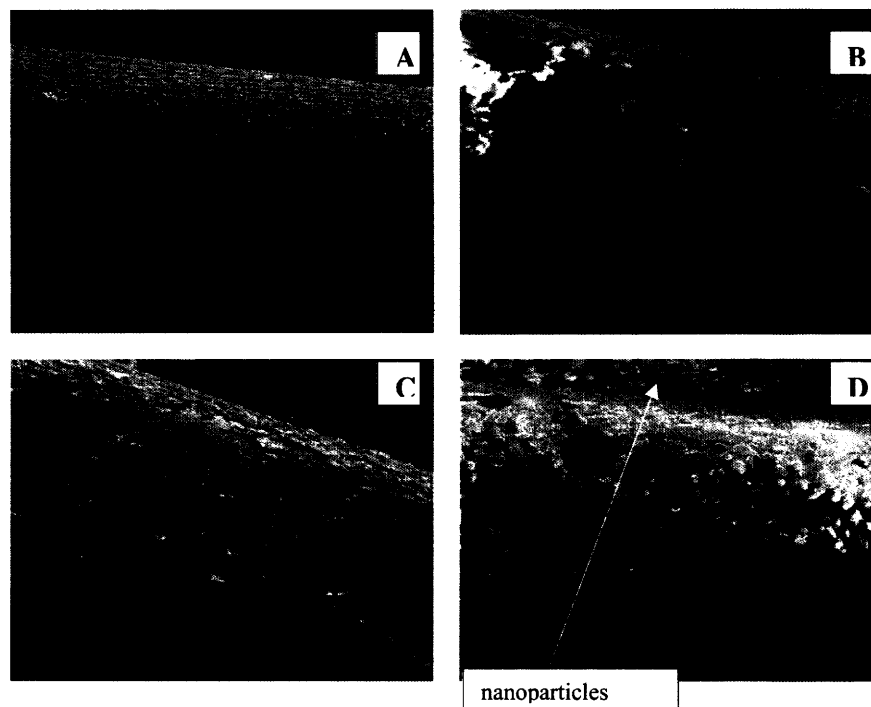


Figure 5-12: SEM image of wires after CHF experiment in A) 0.001 vol%; B, C) 0.01 vol% and D) 0.1 vol% Silica.

In Figure 5-12, notice that the wire in 0.001 vol% Silica is coated by a uniform layer of Silica nanoparticles. Stainless steel wire cannot easily be seen. On the other hand, on the wire in 0.01 vol% or 0.1 vol% Silica, the coating seems sporadic. There are locations where the thickness of the coating is much larger compared to that in 0.001 vol% Silica case. However, there are spots where the base wire can be seen. Saturation thickness for the deposition of the nanoparticles can explain for such observation. Once the thickness of the layer passes this saturated point, the layer may become too heavy to be attached to the wire and it falls off during the CHF experiment or just during the handling of the wire for SEM. In fact, in Figure 5-12: D, there are some particles (white spots) next to the wire can be observed at the top of the picture. These must have fallen off the wire while the wire was being attached to the SEM base, which demonstrates how easy the particle can fall off, and this confirms earlier observation in Figure 5-11 that Silica particles on the wire's surface fall off relatively easy. This means that there must be a saturated point for deposition of the particles during the process of nucleate boiling. In order to study surface treatment using nanoparticle deposition and its limit, flat plate heater is recommended.

5.2.2 Thickness of Nanoparticle Deposition

From the SEM thickness measurement of the particle deposition, one can approximate the amount of the particle deposition as followed. Assuming the coating layer is of uniform thickness, the amount of Alumina nanoparticles deposited can be calculated as:

$$m_{partilce} = \rho_{particle} \frac{\pi}{4} ((d_{wire} + t)^2 - d_{wire}^2) * L, \quad (5-1)$$

where t is the estimated layer's thickness, L is the length of the wire, d_{wire} is the wire diameter. Figure 5-13 below shows the amount of nanoparticles deposited on the wire assuming uniform thickness with 3% porosity.

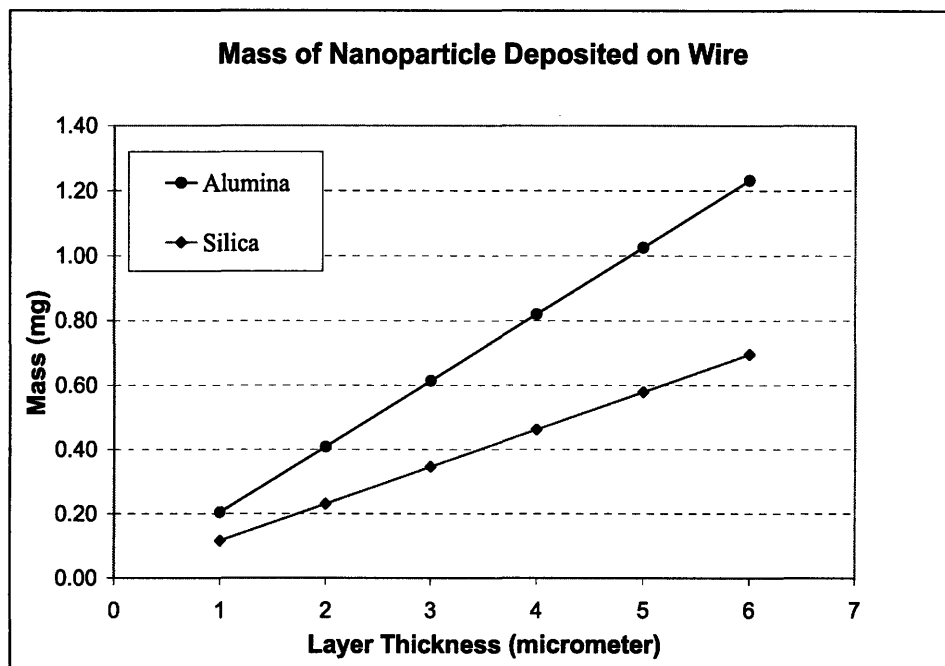


Figure 5-13: Theoretical calculation for mass of nanoparticle deposited on wire. The calculation assumes uniform coating of nanoparticle on the wire and 3% porosity.

The amount of particle deposited, therefore, is too small to be weighted since the mass of the piece of wire is much larger than that of the particle deposited. One other attempt to quantify the amount of the nanoparticle deposited is to use Inductively Coupled Plasma – Optical Emission Spectrometer (ICP-OES). ICP-OES works on the basis that each element emits light with a characteristic wavelength. Basically an ICP torch excites the elements going through it. Subsequently the elements release their excitation energy through light emission, which can be detected by the OES.

Since the nanoparticles are deposited on the wire with only micrometers thickness, scraping the particles off the wire can cause loss of particles due to their volatility. Therefore, the wire (approximately 8.5 cm) with nanoparticle deposited on surface was dissolved in 2 ml of aqua regia, a solution made of nitric acid, hydrochloric acid and water at volume concentration of 10% to 40% to 50%, respectively. The solution is then diluted with 38 ml of deionized water, which makes 40 ml of solution in total. To make a blank standard, 8.5 cm of bare stainless steel wire was also dissolved in 2 ml of aqua regia of the same composition and was then di-

luted with 38 ml of water. Standards with certain amount of Alumina or Silica (in ppm) were made using the blank standard and the 100 ppm Aluminum and Silica standards, respectively.

The ICP results are shown in Table 5-1.

Table 5-1: ICP results. All experiments where the nanofluid is listed uses a bare stainless steel wire was used as heater to measure CHF of the nanofluid. The thickness is calculated assuming uniform coating.

Type of CHF exp.	Trial 1 (ppm) \pm Std	Trial 2 (ppm) \pm Std	Thickness (μm)
0.001 vol% Alumina	0.098 ± 0.004	0.100 ± 0.004	0.034
0.01 vol% Alumina	0.059 ± 0.004	0.066 ± 0.009	0.020
0.1 vol% Alumina	0.034 ± 0.003	0.056 ± 0.003	0.015
Coated wire in water	0.054 ± 0.002	0.060 ± 0.001	0.019
0.001 vol% Silica	Silica could not be detected due to presence of Silicon (1%) in Stainless steel 316. The strength of the signal is less than the back ground level.		
0.01 vol% Silica			
0.1 vol% Silica			

Notice that the measured concentration by ICP are either non-detectable (for Silica case) or much smaller (for Alumina) compared to the thickness measured by SEM. Several reasons can contribute to such discrepancies. First, the measurement from SEM, which is only taken from one 1cm long segment, is not representative of the entire wire. Secondly, the effective density of the layer is smaller than the bulk density of the nanoparticle material. Thirdly, the nanoparticles might have agglomerated during the deposition process and become micron size. These particles would fall out during ICP measurement and would not be detected and hence gave a lower concentration. However, pH measurement of the diluted aqua regia gave value between 1 and 2, which is acidic enough to dissolve Alumina. Therefore, even if the particles had agglomerated during CHF test, they would have been dissolved completely and detected by ICP. In addition, there are Aluminum and Silicon impurities in the stainless steel wire. The concentration of these impurities can be of the order of the amount of nanoparticle deposited (or sometimes even much larger). For example, Silica deposition (seen and verified by SEM-EDS), could not be detected by ICP because there is somewhere between 0.75 to 1.0% of Silicon, corresponding to 10000 ppm by mass, in stainless steel. This background level is a lot higher than the expected several ppm for deposited Silica. Finally, deposited par-

ticles on the wire can fall out during the whole time between the CHF experiment, SEM images and ICP.

SEM by itself can give reasonable measurement of the thickness of the deposition, and the estimation of the mass. ICP, with the sample prepared in a different way, where the wire is not dissolved and the particles have not agglomerated, can verify SEM measurement as well as provide more quantitative data. Together, the data can be used to approximate the porosity and/or surface roughness of the deposited layer. This analysis is recommended for future work.

5.2.3 Possible CHF Enhancement Mechanisms

- **Hydrodynamic Instability:** The relationship in Equation 3-1 provided by Zuber and Kutateladze [26] states that CHF only depends on the physical properties of the fluid. However, since the nanofluids used for CHF experiments have similar properties to those of water, except for the surface tension of 0.01 vol% and 0.1vol% Alumina nanofluids, whose value is about half of that of water. In Equation 3-1, $q_{CHF} \propto \sigma^{1/4}$, which means that everything else equals, the CHF of the nanofluids should be about 15% lower than that of water. But in fact the CHF of Alumina nanofluids is higher than that of water. No other parameter in the hydrodynamic instability theory can provide explanation of the CHF enhancement in the rest of the nanofluids. Hydrodynamic instability alone, therefore, is not sufficient to explain the enhancement.
- Kim et al. [11] showed that macrolayer dryout, hot/dry spot and bubble interaction CHF theory, all of which relate to the contact angle between the liquid and the heater surface; seems to provide a plausible explanation for CHF enhancement in nanofluids. The deposition of the nanoparticles on flat surfaces decreases the contact angle (verified experimentally in flat heater), which subsequently increases the surface wettability. Improvement in wettability allows more fluid to be supplied to the heater easier,

and hence can help enhance CHF. In fact, Kandlikar [38] provided a model to show the effects of contact angle on CHF, which agrees with many experimental data.

- For the work presented here, all the heaters are wire of diameter 0.381 mm, and we have not found a method or instrument to measure contact angle without large uncertainty. This would definitely be future tasks that need to be performed. Therefore, the mechanisms with contact angle as one of the parameters that affect CHF are not readily applied. However, the surface roughness of the wire boiled in nanofluid definitely increased compare to the wire in water. The changes in surface morphology of the wire appear to be the main cause of CHF enhancement. Hwang and Kaviany [39] showed that pre-treated uniform coating surfaces have 1.8 times higher CHF compared to plain surface. They provided a model to predict CHF in uniform particle coating as

$$q_{CHF} = h_{fg} \left(\frac{2\pi^3 a^3 \sigma \rho_g}{9\lambda_{RT}} \right)^{1/2} \quad (5-2)$$

where $\lambda_{RT} = 9 \left[\frac{\sigma}{g(\rho_l - \rho_g)} \right]^{1/2}$ is the Raleigh-Taylor wavelength, and a is the area of the vapor channel. In Equation 5-2, CHF can increase by either an increase in a or a decrease in λ_{RT} . In this work, λ_{RT} stays relatively constant among the nanofluids due to their similar thermophysical properties compared to water. Therefore, an increase in a is the one left. The wires in our experiments are coated with a layer of nanoparticles as shown in previous SEM images. This coating, though not uniform, is somewhat similar to the treated coating by Kaviany and Hwang [39], which means that it can help to increase vapor channel's area, a , subsequently increases CHF. However, quantitative analysis cannot be done at this point due to lack of vapor channel's area measurement.

- Y. V. Polezhaev et al. [40] also suggested a CHF model for uniform porous-layer coatings as

$$q_{CHF} = 0.52\varepsilon^{2.28} h_{fg} \left[\frac{2\rho_l \rho_g}{(\rho_l + \rho_g) d_{br}} \right]^{1/2} \quad 5-3$$

where ε is the porosity of the coating and d_{br} is the breakthrough bubble diameter (the diameter at which the bubbles penetrate the coating), which are the only two values that can change and affect CHF in our case. The porosity of the wire coated with nanoparticle is higher than that of the plain wire, so CHF can be enhanced (assuming everything else equal) by this nanoparticle coating. Again, the coating of the nanoparticles on the wire seems to explain the enhancement in CHF observed.

5.2.4 Nucleate boiling heat transfer coefficient

Figure 4-5 and Figure 4-8 show that the boiling curves in nanofluids shifted to the left of that in water, which means that the nucleation boiling heat transfer coefficient is also enhanced in nanofluids. While this agrees with Wen and Ding [9] who studied pool boiling heat transfer of Alumina nanofluids, Bang et al. [4] and Kim et al. [11] reported the boiling curves in nanofluids shifted to the right of that of water, which means deterioration in heat transfer in nucleate boiling. On the other hand, Vassallo et al. [6] and You et al. [2] reported no shift in boiling curves in nanofluids. Furthermore, Liter and Kaviaby [41], Hwang and Kaviany [39], and Rainey et al. [42] showed boiling curves on porous surface (similar to wire boiled in nanofluids) are shifted to the left of that of plain surface (similar to wire boiled in water here). Overall, there are still discrepancies in nucleate pool boiling heat transfer in nanofluids. One possible reason is that the nanofluids used by experimenters came from different vendors, who produced the nanofluids differently.

In the work here, the temperature of the wire could not be measured directly and so it was deduced from the wire's resistance based on the temperature coefficient of resistance of

stainless steel, which is small, $0.000774 \Omega/(\Omega\text{-}^\circ\text{C})$. For a change in temperature from saturation of 100°C to 160°C , the wire resistance only changes by approximately 0.0320Ω , which gives a change in resistance of 0.0053Ω for every 1°C change in the wall temperature. This value is small and therefore the measurements of the resistance sometimes are not accurate. The instrument uncertainty of 20 mV in measuring voltage across the wire gives approximately 0.01Ω uncertainty in calculating the wire's resistance. This value is almost two times higher than the change in of the wire resistance per degree Celsius. This, therefore, can introduce large uncertainty in the wire's superheated temperature. In future work, it is recommended that either a different wire material (pure Nickel or Nickel-Chromium alloys), is used so that the change in resistance is significant over the interested temperature range and/or measuring the temperature of the wire (heaters) directly instead of deducing from the resistance.

6 Chapter 6 – Conclusion

Pool boiling CHF using stainless steel wire heater in Silica and Alumina nanofluids of volume concentration less than or equal to 0.1% was found to be higher than that of water. While Alumina nanofluid has a peak CHF value of at 0.01 vol%, Silica's CHF values increase with volume concentrations. Alumina has highest CHF of 1.31 MW/m^2 at 0.01 vol% (56% enhancement) while Silica has 1.41 MW/m^2 maximum CHF at 0.1 vol% (68% enhancement). Mechanism for such difference between the nanofluids still needs to be identified. SEM images of the wire heaters confirm the deposition of the nanoparticles during nucleate boiling, which causes changes in the surface's morphology. The coating pattern is found to be consistent within the same fluid. The thickness of the coating layer was found to be of the order of several micrometers for Alumina and as high as 20 micrometer for Silica and this gives an estimation for the amount of nanoparticles deposited on the heaters. ICP-OES was found not effective in quantifying the mass of the particle deposited.

The Hydrodynamic instability model alone is not sufficient to explain the CHF enhancement mechanism of nanofluids as their thermo physical properties are similar to those of water. Mechanisms where CHF depends on the contact angle between the fluid and the heater cannot be readily verified for the small cylindrical wire due to difficulties in measuring contact angle for such geometry. An enhancement mechanism based on coating of a porous layer seems plausible. The wires subject to nanofluids were found to have a porous coating layer of nanoparticles. Quantitative analysis of how such layer affect CHF can be done in the future once the mass and the porosity of the layer deposited on the wire can be measured. Currently, due to the geometry of the wire with small diameter, these types of measurements cannot easily be performed without large uncertainty. Future works include finding different methods and/or instruments to characterize the wire's surface more in depth than SEM can.

Bibliography:

- [1] U.S. DOE and Generation IV International Forum, "A technology roadmap for generation IV nuclear energy systems". Technical report, Department of Energy, Washington D.C, December (2002).
- [2] S. M. You, J. H. Kim, and K. H. Kim. "Effect of nanoparticles on critical heat flux of water in pool boiling heat transfer," *Applied Physics Letters*, 83, 16, 3374–3376, (2003).
- [3] J. Buongiorno, L.W. Hu, S.J. Kim, R. Hannink, B. Truong and E. Forrest, "Uses of Nanofluids for Enhanced Economics and Safety of Nuclear Reactors." *2nd COE-INES International Symposium*, Tokyo, November 26-29, (2006).
- [4] I. C. Bang and S. H. Chang. "Boiling heat transfer performance and phenomena of Al₂O₃ water nano-fluids from a plain surface in a pool." *International Journal of Heat and Mass Transfer*, 48:2407–2419, (2005).
- [5] S. Choi, "Enhancing thermal conductivity of fluids with nanoparticles", in *Developments and Applications of Non-Newtonian Flows*, D.A. Siginer and H.P. Wang (Ed.), ASME, FED-Vol. 231/MD-Vol. 66, 99-105.
- [6] P. Vassallo, R. Kumar, and S. D'Amico, "Pool Boiling Heat Transfer Experiments in Silica-water nanofluids," *International Journal of Heat Transfer*, 47, 407-411, (2004).
- [7] H. Kim, J. Kim and M. Kim, "Experimental Study on CHF Characteristics of Water-TiO₂ nanofluids", *Nuclear Engineering Technology*, 38, 1, 61-68, Feb, (2006).
- [8] R. Kumar, D. Milanova, S. Kuchibhatla and S. Seal, "Heat Transfer Behavior of Oxide Nanoparticles in Pool Boiling Experiment, " *Proceedings of ASME 2006, 4th International Conference on Nanochannels, Microchannels and Minichannels*, Limerick, Ireland, June 19-21, (2006).
- [9] D. Wen and Y. Ding, "Experimental Investigation into the Pool Boiling Heat Transfer of Aqueous Based γ -alumina nanofluids," *Journal of Nanoparticle Research*, 7, 265-274, (2005).
- [10] S. K. Das, N. Putra, and W. Roetzel, "Pool Boiling Characteristics of nano-fluids", *International Journal of Heat and Mass Transfer*, 46, 851-862, (2003).
- [11] S. J. Kim, I. C. Bang, J. Buongiorno, L. W. Hu, "Surface Wettability Change during Pool Boiling of Nanofluids and its effect on Critical Heat Flux", *Int. J. Heat Mass Transfer* (in press, available online March 26, 2007).
- [12] S. J. Kim, "Static Contact Angle Measurement for the Nanofluids", *Special Problem 22.091*, Department of Nuclear Science and Engineer at Massachusetts Institute of Technology, August (2005).
- [13] Y. Xuan, Q. Li, "Heat Transfer Enhancement of Nanofluids", *International Journal of Heat and Fluid Flow*, 21, 58-64, (2000).

-
- [14] S. Choi, "Nanofluid Technology: Current Status and Future Research", Technical Report, Argonne National Laboratory, (1999).
- [15] Malvern Instrument, "Dynamic Light Scattering: An introduction in 30 minutes", www.malvern.co.uk
- [16] Personal Communication with E. Forrest (MIT), J. Inderdohnen (Brookhaven Instruments Corp.).
- [17] Nyacol Nanotechnology, <http://www.nyacol.com/A120PQ3-99.htm>, (2007).
- [18] Sigma Aldrich, "Ludox TMA Colloidal Silica", <http://www.sigmaaldrich.com/catalog/search/ProductDetail/ALDRICH/420859> (2007).
- [19] R. Rusconi, L. Isa, and R. Piazza, "Thermal-lensing measurement of particle thermophoresis in aqueous dispersions", *J. Opt. Soc. Am. B*, 21, 3, 605-616, (2004).
- [20] KVS Instruments, <http://www.ksvltd.com/content/index/sigma703D>", (2007).
- [21] Decagon Device, "<http://www.decagon.com/aw/kd2>" (2007).
- [22] Cannon Instrument, "<http://www.cannoninstrument.com/>", (2007).
- [23] CRC Handbook of Chemistry and Physics, NIST, 87th Edition, (2006 -2007).
- [24] N. Nukiyam, "The maximum and minimum value of heat transfer q transmitted from metal to boiling water under atmospheric pressure", *Int. J. Heat Mass Transfer*, 9, 1419-1433, (1966).
- [25] F. Incopera, D. Dewitt, T. Bergmann and A. Lavine, "Fundamental of Heat and Mass Transfer", 6th Edition, Chapter 10, John Wiley & Sons, Hoboken, NJ, (2007).
- [26] S. S. Kytaleladze, "On the transition to film boiling under natural convection", *Kotloturbostroenie*, 3, 10, (1948).
- [27] J. Lienhard IV, J. Lienhard V, "A Heat Transfer Textbook", 3rd Edition, Phlogiston Press, Cambridge, MA, (2006).
- [28] N. Zuber, "On the Stability of boiling heat transfer", *Trans. ASME. J. Heat Transfer*, 80, 3, 711 – 720, (1958).
- [29] Y. Katto, S. Yokoya, "Principal Mechanism of Pool Boiling on a Horizontal Surface", *International Journal of Heat and Mass Transfer*, 11, 17-29, (1968).
- [30] Y. Haramura and Y. Katto, "A New Hydrodynamic Model of Critical Heat Flux, Applicable Widely to Both Pool and Forced Convection Boiling on Submerged Bodies in Saturated Liquids", *Int. J. Heat Mass Transfer*, 26, No. 3, 389-399, (1983).

-
- [31] Y. H. Zhao, T. Masuoka, T. Tsuruta, "Unified Theoretical Prediction of Fully Developed Nucleate Boiling and Critical Heat Flux Based on a Dynamic Microlayer Model", *Int. J. Heat Mass Transfer*, 45, 3189-3197, (2002).
- [32] S. M. You, Y. S. Hong and J. P. O'Connor, "The Onset of Film Boiling on Small Cylinders: Local Dryout and Hydrodynamic Critical Heat Flux Mechanisms", *Int. J. Heat Mass Transfer*, 37, 16, 2561-2569, (1994).
- [33] J. H. Lienhard and K. H. Sun, "Peak Boiling Heat flux on Horizontal Cylinder", *Int. J. Heat Mass Transfer*, 13, 1425-1439, (1970).
- [34] J. H. Lienhard, N. Bakhru, "Boiling From Small Cylinders", *Int. J. Heat Mass Transfer*, 15, 2011-2025, (1971).
- [35] S. J. Kim, "Boiling Point Measurement for Nanofluids", *Special Problem Report 22.902*, MIT, (2005).
- [36] <http://hyperphysics.phy-astr.gsu.edu/hbase/electric/restmp.html>
- [37] W.M. Rohsenow, "A Method of Correlating Heat Transfer Data for Surface Boiling Liquids", *Transactions of ASME*, Vol.74, pp. 969-976 (1952).
- [38] S. G. Kandlikar, "A theoretical Model to Predict Pool Boiling CHF Incorporating Effects of Contact Angle and Orientation", *J. Heat Transfer*, 123, 1071-1079, Dec. (2001).
- [39] G. S. Hwang, M. Kaviany, "Critical Heat Flux in Thin, Uniform Particle Coatings", *Int. J. Heat Mass Transfer*, 49, 844-849, (2006).
- [40] Y. V. Polezhaev, S. A. Kovalev, "Modeling Heat Transfer with Boiling on Porous Structures", *Therm. Engineering*, 37(12), 617-620, (1990).
- [41] S. G. Liter and M. Kaviany, "Pool-boiling CHF enhancement by modulated porous-layer coating: theory and experiment", *Int. J. Heat Mass Transfer*, 44, 4287-4311, (2001).
- [42] K. M. Rainey, S. M. You and S. Lee, "Effect of Pressure, Subcooling and Dissolved Gas on Pool Boiling Heat Transfer from Microporous Surfaces in FC-72", *J. Heat Transfer*, 125, 75-83, (2003).